Numerical Investigation of Vortex Generator and Jet in Cross-Flow Enhancements

by

ADITYA RAMAN

Presented to the Faculty of the Graduate School of

The University of Texas at Arlington in Partial Fulfillment

of the Requirements

for the Degree of

DOCTOR OF PHILOSOPHY

THE UNIVERSITY OF TEXAS AT ARLINGTON

December 2016

To my parents,

Lata Raman and Late V.S. Raman,

my sister,

Apurva Raman

And my grandParents

ACKNOWLEDGEMENTS

I express my sincere gratitute to my supervising professor Dr. Brian Dennis for giving me the opportunity with all the requisite resources and an evironment to learn and grow. I thank you for your insightful suggestions and advice, it has really shaped the way I think and approach a problem. I value all that I have learned from you.

I would like to thank Dr. Donald Wilson, Dr. Zhen Han, Dr. Ratan Kumar and Dr. Guojun Liao for taking time out to be a part of my committee. Your suggestions and critique was very valuable and has helped me improve my work.

I thank all my colleagues from Computational Fluid Dynamics Lab (CFDLAB) for their support and inspiration. I truly cherish all the discussions and conversations I've had with all of you.

I would also like to thank all family members and friends for encouraging me to dream big and work hard to achieve those dreams.

I am thankful to my sister for her support and motivation. I would also like to thank Reema Desai for understanding and tolerating my frustrations.

I am extremely grateful to my mother for all the sacrifices she's made on my behalf. Thank you for being a pillar of strength, you have always been the light guiding me in the dark. This wouldn't have been possible without your support.

December 13, 2016

ABSTRACT

Numerical Investigation of Vortex Generator and Jet in Cross-Flow Enhancements

ADITYA RAMAN, Ph.D.

The University of Texas at Arlington, 2016

Supervising Professor: Brian H Dennis

Vortex generators have extensively been used over the past few decades for heat transfer applications. Their passive form of enhancement coupled with the ease of their implementation is the primary reason for their growing popularity. The streamwise counter rotating vortex pair (CVP) that is formed downstream of these vortex generators act as a source of energy that can set up stirring scales to enhance heat transfer and improve mixing. The CVP can be used to energize the boundary layer in the case of wall bounded flows, and as a consequence vortex generators have also been used to delay flow separation. A lot of work has been done to determine the extent of the enhancement and to maximize it but not much work is done to study the mechanism. Recent design optimization studies report multiple optimal configurations that maximize the heat transfer enhancement. It is well understood that the CVP is the primary source of all vortex generator based enhancements and a detailed study of the CVP and its interaction with the boundary layer is thus beneficial to improve design considerations.

Another means of heat and mass transfer enhancement that is often used is the jet in cross-flow. A jet issued into the cross-flow has distinct flow features along

with a longitudinal CVP that serve as a means of enhancement. In contrast to the vortex generators, a jet in cross-flow is an active means of enhancement as it requires external power to pump the jet. The jet in cross-flow has numerous applications, including but not limited to

- Mixing of fuel & air in a combustion chamber;
- Turbine blade film cooling;
- Jet impingement heat transfer enhancements;
- Thrust vectoring

The jet in cross-flow is a well studied problem and a lot of qualitative and quantitative data is available for this application. Direct numerical simulations (DNS) and Experimental studies have well established the means of enhancement in this field of study. Researchers have also studied the stability characteristics of the jet in cross-flow and found it to be absolutely unstable. The flow transitions to turbulent which is beneficial as it enhances the mixing characteristics and heat transfer.

In this research, the effect of geometric and flow parameters of a passive delta winglet vortex generator like the vortex generator angle of attack, Reynolds number and the undisturbed boundary layer height on the heat transfer enhancement and vortex strength is studied. The time averaged effect of the vortex shedding on the heat transfer enhancement is quantified. The vorticity transport equation is used to identify the sinks of vorticity with a goal to gain a better understanding of the enhancement mechanism and the vortex interaction with the boundary layer. The mixing efficiencies of the vortex generator employed along with a jet in crossflow is compared to the baseline case without the vortex generator.

TABLE OF CONTENTS

ACKNOWLEDGEMENTS iv

ABSTRACT v

LIST OF FIGURES ix

LIST OF TABLES xiii

Chapter Page

1. INTRODUCTION 1

1.1 Vortex Generators 1

1.2 Literature Review of vortex generators 3

1.3 Jet in Cross-Flow 6

1.4 Literature Review of a Jet in Cross-Flow 7

1.5 Research Objectives and Contributions 9

1.6 Dissertation Organization 10

2. VORTEX GENERATORS 12

2.1 Preliminary Study 12

2.1.1 Computational Domain & Mesh 12

2.1.2 Numerical Methodology 13

2.1.3 Results & Discussion 16

2.1.4 Validation of the use of slip boundary condition 23

3. EFFECT OF BOUNDARY LAYER HEIGHT ON THE VORTEX CIRCULATION & HEAT TRANSFER 26

3.1 Methodology 26

3.2 Results 28

4. VORTICITY TRANSPORT 32
4.1 Derivation of the Vorticity Transport Equation 32
4.2 Methodology 35
4.3 Results & Discussion 36
5. INFLUENCE OF SHEDDING ON HEAT TRANSFER ENHANCEMENT 46
5.1 Computational Domain and Mesh 47
5.2 Reynolds - Strouhal Number Relationship 48
5.3 Effects on Heat Transfer 49
6. VORTEX GENERATOR WITH JET IN CROSS-FLOW 52
6.1 Preliminary Study of the Jet in Cross-flow 52
6.1.1 Computational domain & Mesh 52
6.1.2 Numerical Methodology 53
6.1.3 Results & Discussion 54
6.2 Vortex Generator along with Jet in Cross-flow 57
6.2.1 Computational Domain & Mesh 57
6.2.2 Numerical Methodology 57
6.2.3 Results & Discussion 58
7. CONCLUDING REMARKS 61
7.1 Summary 61
7.2 Future Work 62
REFERENCES 63
BIOGRAPHICAL STATEMENT 68

LIST OF FIGURES

Figure Page

1.1 Figure showing the common configurations of the delta-winglet vortex generators, taken from Jacobi & Shah [1] 2

1.2 The canonical jet in cross-flow, taken from Muppidi & Mahesh [2] . . 6

2.1 Figure showing the Computational domain and mesh for the vortex generator 12

2.2 Probe data showing convergence to steady state 15

2.3 Average Nusselt number variation 17

2.4 Variation of vortex circulation with the streamwise direction 19

2.5 Average Circulation variation with Reynolds number and Angle of attack 19

2.6 Variation of the streamwise content of vorticity in the boundary layer in the streamwise direction 20

2.7 Isolated vorticity contours around the vortex at different spanwise sections 21

2.8 Isolated vorticity contours around the streamwise vorticity in the boundary layer at different spanwise sections 22

2.9 Vortex center positions for $\alpha = 15°$ 22

2.10 Vortex center positions for $\alpha = 30°$ 23

2.11 Domain and mesh considered to validate the use of slip boundary condition 24

2.12 Contour of velocity component normal to the plane 24

2.13 Effect of slip wall boundary condition on the circulation 25

3.1 Figure showing the inlet velocity contour and profile for the micro vortex generator cases 27

3.2 Average Nusselt number ratio variation 28
3.3 Average Circulation variation 29
3.4 Comparison of the streamwise variation of the circulation 30
3.5 Streamwise variation of the vortex circulation for the micro vortex generator 30
3.6 Streamwise variation of the boundary layer circulation for the micro vortex generator 31
4.1 Figure showing the vorticity fluxes of the macro vortex generators for $Re = 750; \alpha = 15^\circ$ 36
4.2 Figure showing the vorticity fluxes of the micro vortex generators for $Re = 750; \alpha = 15^\circ$ 37
4.3 Figure showing the vorticity fluxes of the macro vortex generators for $Re = 1000; \alpha = 15^\circ$ 38
4.4 Figure showing the vorticity fluxes of the micro vortex generators for $Re = 1000; \alpha = 15^\circ$ 39
4.5 Figure showing the vorticity fluxes of the macro vortex generators for $Re = 1250; \alpha = 15^\circ$ 39
4.6 Figure showing the vorticity fluxes of the micro vortex generators for $Re = 1250; \alpha = 15^\circ$ 40
4.7 Figure showing the vorticity fluxes of the macro vortex generators for $Re = 1500; \alpha = 15^\circ$ 40
4.8 Figure showing the vorticity fluxes of the micro vortex generators for $Re = 1500; \alpha = 15^\circ$ 41
4.9 Figure showing the vorticity fluxes of the macro vortex generators for $Re = 750; \alpha = 30^\circ$ 41

4.10 Figure showing the vorticity fluxes of the micro vortex generators for $Re = 750; \alpha = 30°$ 42
4.11 Figure showing the vorticity fluxes of the macro vortex generators for $Re = 1000; \alpha = 30°$ 42
4.12 Figure showing the vorticity fluxes of the micro vortex generators for $Re = 1000; \alpha = 30°$ 43
4.13 Figure showing the vorticity fluxes of the macro vortex generators for $Re = 1250; \alpha = 30°$ 43
4.14 Figure showing the vorticity fluxes of the micro vortex generators for $Re = 1250; \alpha = 30°$ 44
4.15 Figure showing the vorticity fluxes of the macro vortex generators for $Re = 1500; \alpha = 30°$ 44
4.16 Figure showing the vorticity fluxes of the micro vortex generators for $Re = 1500; \alpha = 30°$ 45
5.1 $\lambda 2$ criterion isocontour plotted to visualize the vortex shedding 46
5.2 Computational domain and mesh used for the case of $\alpha = 45°$ 47
5.3 Probe data taken for the case of $Re = 750; \alpha = 45°$ 48
5.4 Figure showing the Reynolds number and Strouhal number relationship 49
5.5 Figure showing the heat transfer enhancement comparisons for all the cases 50
5.6 Figure showing the thermal performance parameter trend comparison for all the cases 51
6.1 Cross-section of the mesh used for this study 53
6.2 Figure showing the jet in cross-flow trajectory 55
6.3 Figure showing the instantaneous center plane scalar concentration . . 56

6.4 Figure showing the computational domain and mesh for the vortex generator - jet cases 57
6.5 Figures showing the $\lambda 2$ criterion to visualize the flow-field 59
6.6 Figure showing the normalized mixing efficiency comparison between the Flow-down and Flow-up configurations 60

LIST OF TABLES

Table Page

2.1 NUMERICAL UNCERTAINTIES 16

CHAPTER 1

INTRODUCTION

1.1 Vortex Generators

Heat exchangers in the earlier days relied on increasing the surface area to maximize the Air-Side heat transfer. With the growing need for compact design and minimizing the manufacturing cost, a lot of work was done on heat transfer enhancements. Heat transfer enhancements are typically used to improve the convective heat transfer characteristics of the heat exchangers employed in industrial and commercial apparatus. These enhancements improve the efficiency of the heat exchangers and thereby help reducing their size, power requirement and cost of implementation. The method of enhancement can broadly be classified in two types active and passive. Active enhancements control the secondary flow characteristics at the cost of pumping power. An external power source is required for their operation, and usually rely on surface vibrations,flow pulsations, electrostatic fields or jet injection to provide mechanical mixing for the enhancement. Passive enhancements on the other hand are employed by providing roughened surfaces or by extending surfaces into the flow to augment the primary flow characteristics. Passive enhancement methods have the advantage of low operating and maintenance cost and their cost of implementation can easily be extended to be a part of the manufacturing process. Delta-winglet vortex generators are an example of such passive methods and the object of this study. A delta-winglet vortex generators can be employed in either flow-down or flow-up configuration. The flow-down configuration produces a clock-wise longitudinal vortex over the left winglet while the flow-up configuration produces a counter clock-wise

longitudinal vortex over the left wing. Figure 1.1 shows these respective configurations. The boundary layer thinning for the flow down configuration occurs in between the vortices while for the flow up configuration, it occurs in the outer region. Both these configurations are observed to have similar heat transfer characteristics.

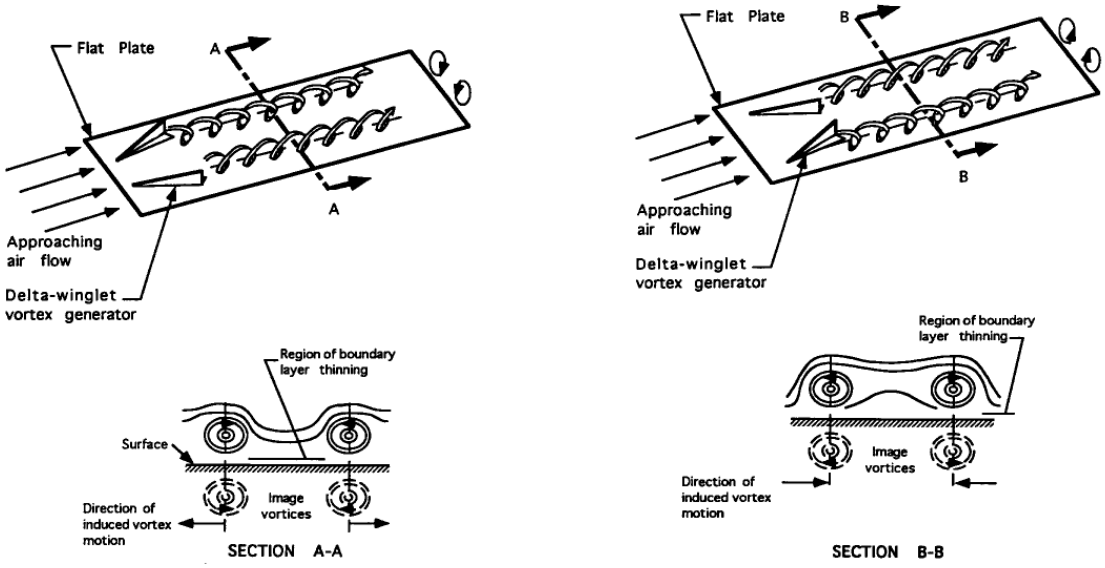

(a) Common Flow Down Configuration

(b) Common Flow Up Configuration

Figure 1.1. Figure showing the common configurations of the delta-winglet vortex generators, taken from Jacobi & Shah [1].

The shearing of the flow due to the obstruction of the vortex generators sets up the longitudinal Counter rotating Vortex Pair (CVP). This then recirculates the free-stream fluid over the heated surface and thus results in the enhancement. The CVP is observed to persist far downstream of the vortex generators and dissipates rather slowly due to its interaction with the boundary layer.

1.2 Literature Review of vortex generators

A comprehensive review of the past work is provided by Jacobi & Shah [1]. Fiebig et al. [3] performed experimental studies on delta-winglet, rectangular-winglet, delta wing and rectangular wing vortex generators in a laminar channel. They found that these enhancement mechanisms provide more than 50% increase in the mean heat transfer characteristics in the channel. They also found that winglets perform better than the wing configurations and that the performance of delta-winglets and rectangular-winglets are similar. The position of the vortex center was reported to be unaffected by the flow Reynolds number and angle of attack but the stability of the vortex seemed to be dependent on Reynolds number and angle of attack. Tiggelbeck et al. [4] performed experimental investigations on aligned rows of vortex generators and reported heat transfer enhancement of 80% along with a drag increase of about 160%. They found that the spacing between the rows plays an important role in the enhancement as for a particular spacing, there seemed to be increased heat transfer enhancement and reduced pressure losses. They employed aligned rows of vortex generators in this study as they found that aligned rows provide greater enhancements that staggered arrays. They reported that the wake flow structure strongly depends on the flow Reynolds number and the angle of attack of the vortex generator as for higher angles of attack, the vortex did not form downstream of the vortex generator. They noted that the critical angle above which the vortex does not form is approximately 70 Deb et al. [5] performed detailed experimental and numerical study on the performance parameters of delta-winglet vortex generators in laminar and turbulent regimes. They used a $k - \epsilon$ model with wall functions for the numerical analysis and found that the average Nusselt number increases with increasing Reynolds number. Gentry & Jacobi [6] studied the possible mechanisms for enhancement and modeled the vortices using simplistic inviscid potential flow theory. They mentioned

the importance of the vortex center height to the undisturbed boundary layer height. If the vortex is far from the boundary layer then there is little enhancement, or if the vortex is embedded within the boundary layer then it dissipates quickly and the mechanism of enhancement thus diminishes. They reported about 50 to 60% increase in the overall enhancement with vortex generators. In a later study Gentry & Jacobi [7] performed vortex measurements to measure the strength of the longitudinal vortices produced and found that it increases with Reynolds number, angle of attack and aspect ratio. They also observed that the vortex decays as it propagates downstream. Sohankar [8] performed large eddy simulation (LES) and Direct Numerical Simulation (DNS) to study two aligned rows of vortex generators. They found that the fluid flow and heat transfer after Reynolds number 1000 becomes unsteady. They mentioned that the flow features like horse-shoe vortices are present close to the wall and they convect along with the longitudinal vortices. The Nusselt number and circulation was found to increase with Reynolds number and angle of attack. He et al. [9] employed a V shaped array of vortex generators drawing inspiration from the formation flight of birds and schools of fish. They reported a 25 to 55% increase in the average heat transfer and also noted that the average nusselt number increases with increasing Reynolds number and angle of attack. Fiebig [10] conducted a survey of wing and winglet configurations and found that the enhancement increased upto a maximum limit with an increase in angle of attack and height for a constant aspect ratio vortex generator. Abdollahi & Shams [11] used pareto optimal strategy along with neural networks to optimize the angle of attack of the vortex generators. Salviano et al. [12] used two different methods for optimization of the vortex generator, response surface methodology using neural networks and direct optimization using genetic algorithms. They found that these different methods lead to different optimal configurations both equally effective. They introduced roll angle as a new parameter

for design. A deeper understanding of the interactions between the vortex and the boundary layer is thus key to efficient designs. Jimenez & Moin [13] studied the near wall turbulence transition process. They found that the thin layers of spanwise vorticity is lifted away from the wall and the intermittent regeneration of turbulence is observed to consist of the wrapping of the wall-layer vorticity around a single inclined longitudinal vortex. Marshall [14] used a quasi 2d approach to study the vortex in unbounded and wall bounded flows. He used a model with vanishing gradients in the streamwise direction which is usually observed for wall bounded vortices. He reported that a region of streamwise vorticity is formed along the walls immediately under the vortex and convects with it. The interaction between the two was reported to be similar to the transition mechanism discussed by [13]. He found that for higher Reynolds numbers, this streamwise vorticity near the wall is ejected from the wall and wraps around the vortices. Wendt [15] performed a parametric study of the vortices shed from airfoil vortex generators and found that the lamb vortex model gives good qualitative agreement with the observed behavior of wall bounded vortices. He also found that the vortex circulation is proportional to the Reynolds number, angle of attack of the vortex generator and the ratio of the vortex generator aspect ratio to the undisturbed boundary layer height. Jukes & Choi [16] studied the formation of streamwise vortices by plasma vortex generators and found the mechanism similar to that of the vortex generators with the only difference being in the enhanced circulation of the plasma vortex generators due to the addition of vorticity in the plasma jet. They proposed scaling laws for the vortex trajectory and observed that the CVP formed closer to the wall.

1.3 Jet in Cross-Flow

The term jet in cross-flow refers to the flow field observed when a jet of fluid exits an orifice and interacts with the surrounding fluid flowing across the orifice. Figure 1.2 shows a schematic of the jet in cross-flow. This type of flow field is common both in nature and also in man made devices. Volcanic eruptions resulting in jet plumes is an example of a naturally occurring phenomenon. The crosswind carries volcanic ash, smoke and other volcanic matter miles away and it of interest to study this flow-field in order to predict the transport of the passive scalar with the jet. Dilution holes for mixing fuel and air inside a supersonic combustor, smoke emitted out of an industrial chimney, thrust vectoring and turbine blade film cooling are some of the man made applications in which the jet in cross-flow is observed.

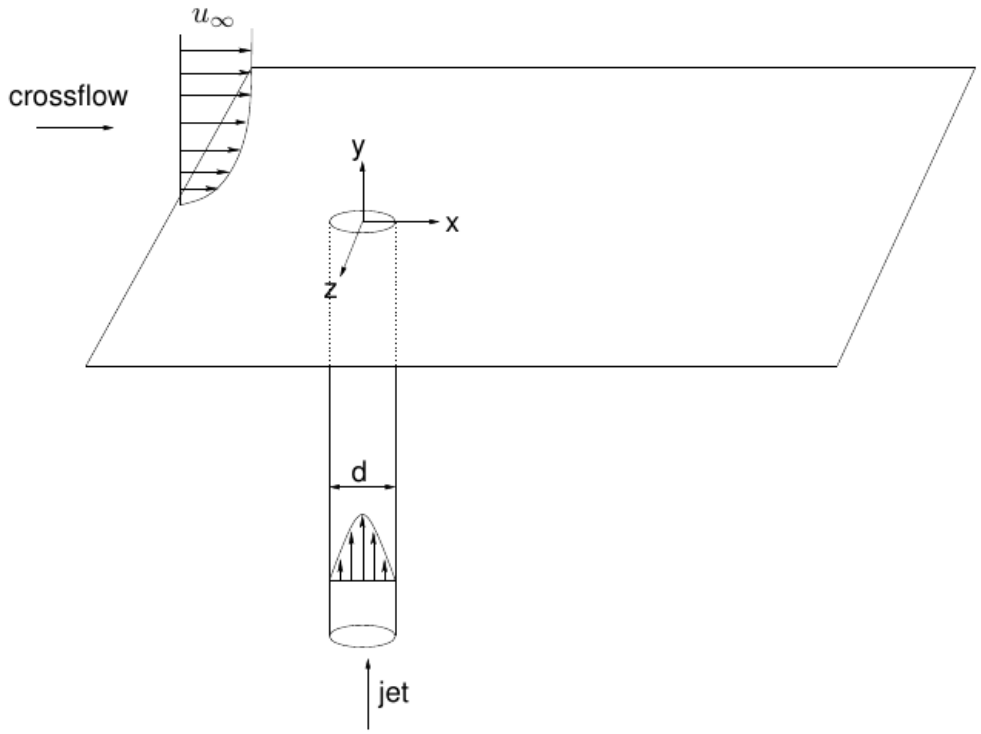

Figure 1.2. The canonical jet in cross-flow, taken from Muppidi & Mahesh [2].

Jet in cross flow is an active method of enhancement that is employed by pumping a jet into the cross flowing stream. It is used for both heat and mass transfer enhancements. Jet impingement heat transfer is an example of the former in which a jet is made to impinge on the surface that needs to be cooled. Non dimensional parameters like the jet velocity ratio and momentum ratio is commonly used to analyze the jet in cross-flow. If the cross-flow and the jet are the same fluid then the velocity ratio i.e. the ratio of velocity of jet to the velocity of the cross-flow is considered as a parameter, while for cases where the two are different, the momentum ratio i.e. the ratio of the jet momentum to the cross-flow momentum is considered. Additional parameters that effect the flow-field are the jet Reynolds number, cross-flow boundary layer thickness to the jet diameter and the velocity profiles of the jet and the cross-flow boundary layer. The interaction of the jet with the cross-flow is unsteady and complex. A number of flow features both in the near and far field are associated with this flow and is a subject of great interest.

1.4 Literature Review of a Jet in Cross-Flow

A detailed review of the flow parameters and the current work is presented by Mahesh [17]. Earlier works in this field examined scaling laws for the mean jet trajectory and the decay of a passive scalar in the jet. Pratt & Baines [18] proposed a length scale of rd where r is the velocity ratio of the jet and d is the jet orifice diameter. Smith & Mungal [19], Su & Mungal [20] and Shan & Demotakis [21] studied the passive scalar mixing in the jet. Smith & Mungal [19] proposed different scaling laws for different regions in the flow field. They found that the jet scales with d in the vortex interaction region where the boundary layer separation occurs, both the near and far field scale with rd. Shan & Demotakis [21] observed that the turbulent mixing in the far field of the transverse field is Reynolds number

dependent as the scalar field probability distribution function (PDF) was found to evolve with Reynolds number. They also found the scalar field to be anisotropic even at smaller length scales. They showed that this anisotropy is correlated to the vortex induced large scale strain field of the transverse jet. Andreopoulos & Rodi [22] performed experimental measurements using a three sensor hot-wire probe and were able to provide a quantitative picture of the complex three dimensional mean flow and turbulence fields. Karagozian [23] developed an analytical model of the CVP associated with the jet in cross-flow. She found that the vortex separation and other important characteristics of the jet cross section are locally two dimensional and viscous in nature. Muppidi & Mahesh [2], performed DNS simulations to study the turbulence quantities. They found that in the near field, peak kinetic energy is observed close to the leading edge, while peak dissipation is observed towards the trailing edge of the jet. They also mentioned that this complex variations make Reynolds Averaged Navier Stokes (RANS) model prediction more difficult. Bagheri et al. [24] performed global stability analysis of the jet in cross-flow. They found that the jet in cross-flow is globally unstable, with self sustained global oscillations for a velocity ratio of 3. They identified the high frequency global eigenmodes associated with the shear layer vortices and the low frequency eigenmodes associated with the shedding in the wake. Karagozian [25] studied the stability characteristics of the jet shear layer as a means to explain the jet response to altered types of excitation. The jet shear layer for higher momentum flux ratios is observed to be convectively unstable while at lower momentum flux ratios it transitions to absolutely unstable behavior. The author noted the effect these stability characteristics have on optimal employment of external excitation to control the jet penetration and spreading characteristics. She also makes a note of the important question in this regard that are still unanswered,

like Is absolutely unstable jet in cross-flow better mixed than the convectively unstable one?

Zaman & Foss [26] performed experimental investigations on the effects of vortex generators on the penetration and spreading characteristics of a jet in cross-flow. They found that the vortex generator has very little effect on the jet when placed on the down stream side of the jet. They also observed that the jet penetration depth either increased or decreased depending on the sense of vorticity being generated by the vortex generator. Van Buren et al. [27] studied the interaction of vortex generator and a synthetic jet in cross-flow. They found that the two CVPs associated with the two devices did not merge. When the vortex generator was placed upstream of the jet, the jet pushed the CVP of the vortex generator upwards and when the vortex generator was placed downstream of the jet, the associated CVP of the vortex generator was completely destroyed. They noted that placing the vortex generator upstream of the jet was imperative to their combined performance. Wang et al. [28] used a similar model for jet impingement heat transfer application. They found that the common flow-up configuration of the vortex generators promotes jet penetration and augments the impingement heat transfer. They also noted that there is an optimal value of the spacing between the vortex generator and the jet orifice. If the vortex generator is too close to the jet orifice, the heat transfer enhancement is reduced and if the vortex generator is too far from the orifice, the impingement becomes weaker owing to the slow decay of the CVP. A further detailed study into these interactions can help design these hybrid actuators much better.

1.5 Research Objectives and Contributions

Most of the previous work on vortex generators focused mainly on quantifying the extent of the enhancement observed for various configurations of the vortex gener-

ators and to qualitatively describe the effects of the vortex interactions. A few design optimization studies have also been carried out recently, however a quantitative description of the vortex boundary layer interaction and its effect on the enhancement is still lacking. And although the topic of jet in cross-flow is extensively studied and improvements in numerical and experimental facilities have made it possible to quantitatively describe the unsteady 3-d turbulent features, not much study is done for the combined use of these two mechanisms and their interactions. Specifically this work focusses on answering the following questions

I. How does the vortex generator parameters affect the vortex circulation ?
II. How does the boundary layer height affect the heat transfer enhancement ?
III. What effect does the vortex shedding has on the heat transfer ?
IV. How does the vortex interact with the boundary layer and what are the sources and sinks of vorticity ?
V. In what way does the vortex generator influence the jet in cross-flow ?

In this work the effect of the vortex generator parameters on the vortex circulation is analyzed. The effect of vortex shedding on the heat transfer enhancement is quantified. The effect of boundary layer height on these parameters is studied and its effect on the heat transfer enhancement is quantified. The vorticity transport equation is used to identify the sources and sinks of vorticity for the vortex, and also to quantify the interaction of the vortex with the boundary layer. The influence of the vortex generator on the jet in cross-flow enhancement is studied.

1.6 Dissertation Organization

Chapter 2 describes the preliminary work done to study vortex generators. This chapter describes the methodology, validation and the preliminary results obtained for the vortex generator.

In chapter 3, the effect of increased boundary layer on the flow characteristics and heat transfer performance of the vortex generator is addressed.

Chapter 4 focuses on the derivation of vorticity transport equation, the methodology used to compute the terms involved in the equation and the observed results for the vortex generator. Results are also presented for the case of increased boundary layer height.

Chapter 5 analyzes the influence of shedding on the heat transfer enhancement of vortex generators and presents the Reynolds number - Strouhal number relationship observed.

Chapter 6 addresses the interaction of the vortex with the jet in cross-flow and its effect on the mixing enhancement. The First half of this chapter describes the preliminary work done to validate the jet in cross-flow application. The second half describes the methodology and results obtained for the vortex generator - jet enhancement.

Chapter 7 gives a summary of all the work done and presents the future direction of this research.

CHAPTER 2

VORTEX GENERATORS

2.1 Preliminary Study

2.1.1 Computational Domain & Mesh

Taking into consideration the symmetry of the vortex generators, only half of the domain was considered for the numerical simulations. This reduces the computational demands and simplifies the analysis. Figure 2.1 shows the simulated computational domain and the mesh.

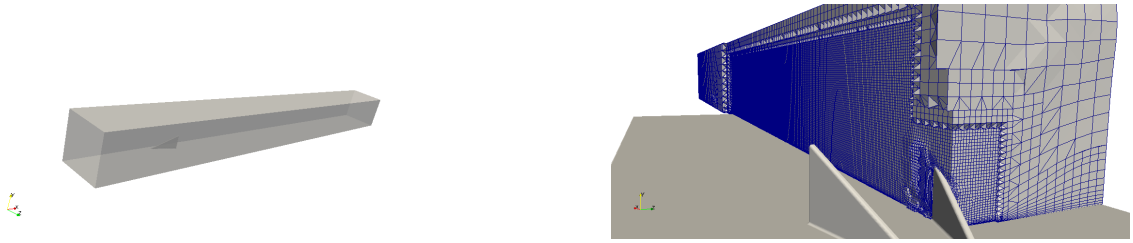

(a) Computational Domain (b) Mesh used for the study

Figure 2.1. Figure showing the Computational domain and mesh for the vortex generator.

The studied domain in Figure 2.1(a) has dimensions $0.7 \times 0.1 \times 0.1m^3$, which is further extended by $0.4m$ in the streamwise direction so as to prevent flow reversal near the region of interest. The length and height of the vortex generator was fixed to be $0.06m$ and $0.03m$ respectively, thereby giving an aspect ratio of 2. The delta-winglet was placed at a distance of $0.16m$ from the inlet region to allow for the flow to develop.

The mesh was generated in an OpenFOAM® mesh generation utility called snappyHexMesh. snappyHexMesh uses an iterative algorithm to mesh the domain of interest. At each refinement or layer addition step, the utility checks the overall mesh quality and takes corrective steps or smoothes the mesh. The end result of this is a hex-dominant high quality mesh. The mesh had more than 95% hexahedral cells with some tetrahedral cells in between the refinement layers as is seen in the Figure 2.1(b). The mesh contained about 1.3 to 2 million cells and a boundary layer mesh over the bottom plate and the vortex generator was also created. A preliminary analysis on a coarse mesh was done to determine the extent of the vortex in the wake region and the cells in this region were then refined to capture all the flow features.

2.1.2 Numerical Methodology

The plate and the vortex generator were given a no-slip boundary condition and a constant heat flux, the central plane was given a symmetric boundary condition and the side and top walls were modeled as slip walls. The use of slip wall is validated in the later part of this chapter. The inlet plane was given a velocity inlet boundary condition with velocity computed from the Reynolds number based on the winglet cord length. Temperature at the inlet was fixed at $300K$ and the pressure was initialized with a zero gradient boundary condition. The velocity at the outlet was given a Dirichlet condition if the flux at the outlet was directed into the domain and a Neumann condition if the flux was directed outside. The pressure at the outlet was fixed at $1atm$ while the temperature was given a zero gradient boundary condition.

The flow simulations were conducted in OpenFOAM® [29], which employs finite volume analysis for solving the incompressible Navier-Stokes equations. The governing equations for incompressible flow are:-

$$\frac{\partial u_i}{\partial t} + u_j \frac{\partial u_i}{\partial x_j} = -\frac{1}{\rho}\frac{\partial p}{\partial x_i} + \nu \nabla^2 u_i \tag{2.1}$$

Along with the continuity equation given by,

$$\frac{\partial u_i}{\partial x_i} = 0 \tag{2.2}$$

And the energy equation

$$\frac{\partial T}{\partial t} + u_i \frac{\partial T}{\partial x_i} = \frac{\nu}{Pr} \nabla^2 T \tag{2.3}$$

Where u is the velocity of the fluid element, ρ is its density, p is the pressure, T is the temperature, Pr is the Prandtl number and ν is the kinematic viscosity. The viscous dissipation terms are neglected. For incompressible flows, the energy equation is independent of the momentum and can be solved as the transport of a passive scalar.

Steady state results were obtained using the S.I.M.P.L.E. Scheme [30]. The convection terms in the Navier-Stokes equations were discretized using a second order upwind scheme and a second order central difference scheme was used for the diffusion terms. Consistent with the observations observations of [8], the flow becomes unsteady for a couple of cases with angle of attack 30° and Reynolds number above 1000. For these cases it became necessary to solve the unsteady Navier-Stokes equations and time march the solution to steady state. The unsteady simulations in these cases were run using the P.I.S.O. Algorithm [31]. Time data was saved for several probes added in the vortex wake at different streamwise locations. The probe data as shown in Fig 2.2 confirms that the solution is indeed steady.

With an objective to provide a measure of error or uncertainty of grid convergence, Roache's [32] Grid Convergence Index (GCI) methodology is used. This

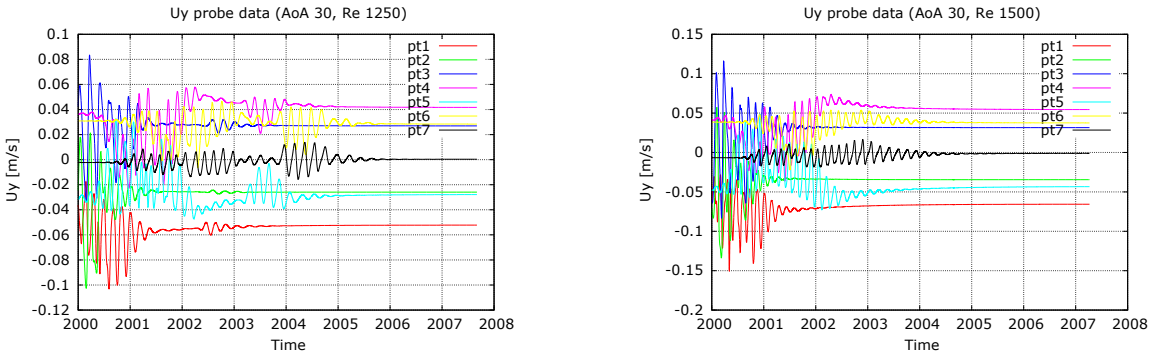

(a) Probe data for Re = 1250

(b) Probe data for Re = 1500

Figure 2.2. Probe data showing convergence to steady state.

method is based upon the grid convergence error estimator derived from the theory of Richardsons Extrapolation. It serves as an error band and also provides an indication of the solution change with further refinement. A small value of CGI indicates that the solution lies in the asymptotic range of convergence and would not change considerably with further refinement. Based on the current mesh used in this study, a coarser mesh with about $150,000$ cells and a much finer one with about 9.4 million cells were considered to estimate the CGI. This gives a ratio of cells between the meshes to be equal to roughly around 7. First the order of the convergence rate is calculated as follows

$$p = \frac{\ln[(\phi_m - \phi_c)/(\phi_f - \phi_c)]}{\ln r} \tag{2.4}$$

Where p is the convergence rate, ϕ represents the solution and the subscripts c, m, f signify the medium, coarse and fine meshes considered and r is the refinement ratio of cells between the meshes.

The discretization error can then be estimated as

$$\epsilon = \|(\phi_f - \phi_m)\|/[r^p - 1] \tag{2.5}$$

The CGI is then calculated by multiplying the error with a factor of safety 3. The following table 2.1 lists the errors associated with the predicted quantities.

Table 2.1. NUMERICAL UNCERTAINTIES

Quantity	GCI (%)
Nu	± 0.1896
Γ	± 0.05878
y_c	± 3.01272
z_c	± 0.2634336

Here Γ is the vortex circulation, Nu is the average nusselt number ratio, y_c and z_c is the vortex center locations.

2.1.3 Results & Discussion

The average Nusselt number was calculated following the procedure reported in [33]. The area weighted temperature values T_o and T_w were calculated at $x = 0.6m$ i.e. at the exit of the domain of interest and at the plate and wing surfaces. The average power gain by the incoming fluid was calculated using

$$P = \rho A U_\infty C_p \times (T_o - T_i) \tag{2.6}$$

where ρ is the fluid density, A is the cross sectional area, U_∞ is the inlet fluid velocity and T_i is the inlet temperature. The average heat flux can then be calculated as

$$Q = P/A_p \tag{2.7}$$

A_p is the total surface area of the plate and the delta wing. The average heat transfer coefficient is then calculated from the average heat flux using

$$h = Q/(T_w - T_f) \tag{2.8}$$

T_f is the average fluid temperature, obtained by averaging the inlet and outlet area averaged temperatures and T_w is the temperature at the wall. Thus Nusselt number is calculated as

$$Nu = hl/k \tag{2.9}$$

Where l is the characteristic length, in this case the length of the delta wing and k is the thermal conductivity of the fluid. The calculated values were then normalized with the baseline case of a flow over a flat plate. The baseline value was looked up from the existing correlation for Nusselt number. Figure 2.3 shows the variation in average Nusselt number with Reynolds number and angle of attack.

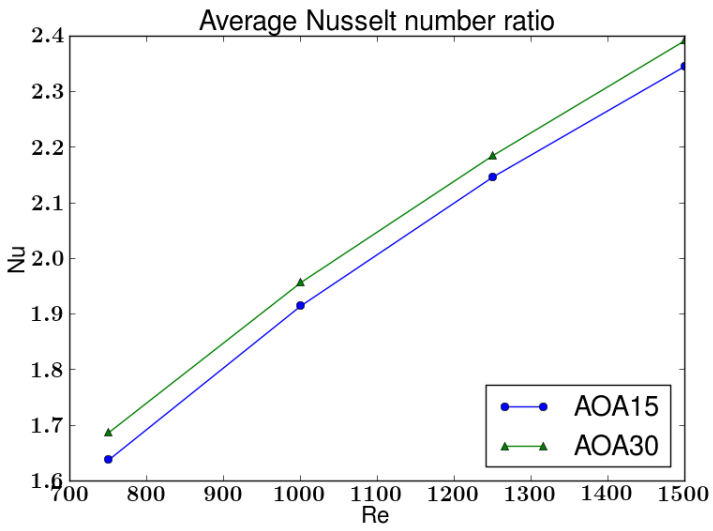

Figure 2.3. Average Nusselt number variation.

Fiebig et al. [3] observed a mean heat transfer enhancement of more than 50%, Gentry & Jacobi [6] reported an enhancement of 50 to 60%, Tiggelbeck et al. [4] observed enhancements of about 80% and the observed values of enhancement in the current work is at least 60% as is seen from Figure 2.3. Also the trends

observed in the current work match the trends reported by Wu et al. [33]. They conducted experimental and numerical investigations and found that the numerical trend matches the experimental trends but the numerical results are under predicted and they attributed this difference to the averaging procedure in the experimental results.

The calculation of vortex circulation in wall bounded flows poses a particular challenge. For free vortex flows, the vortex section is circular and hence it becomes easier to define a circular contour around the vortex to calculate the circulation. Wall bounded vortices on the other hand are not circular and their shape keeps changing in space as they keep interacting with the boundary layer. Here the vortex center location was identified as the region of peak vorticity, an increasing value of cut-off was used to filter the data around the center and the circulation was calculated by taking the dot product with the cell areas and integrating it over the region of cut-off. For increasing values of the cut-off, the circulation was computed and the value was chosen such that it did not change much with the increasing cut-off. This is because any contour slightly outside the vortex edge would not give much change in the circulation. Circulation was calculated at spanwise sections behind the delta wing by extracting the planar data of vorticity and cell areas. This was then normalized by dividing it with $(U_\infty \times l)$ and the non-dimensional values were plotted.

$$\Gamma = \int_A \vec{\omega}.\hat{n}dA \tag{2.10}$$

Figure 2.4 shows the variation in the vortex circulation along the streamwise direction behind the vortex generator. The streamwise location is normalized by the vortex generator length l.

It can be seen from Fig 2.4 that the vortex circulation increases with increasing Reynolds number and angle of attack α. For a given case of Reynolds number and α,

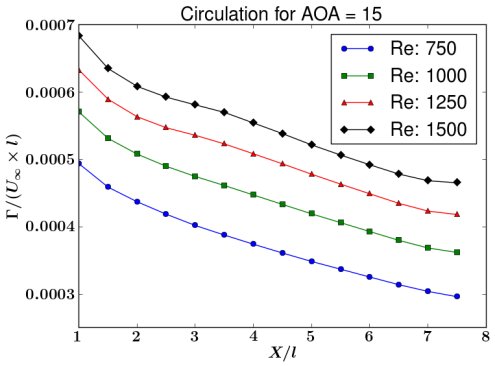

(a) Circulation for angle of attack 15

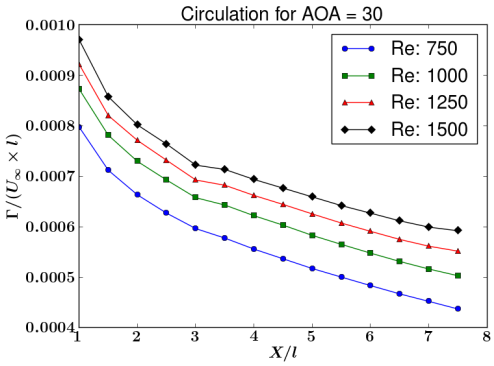

(b) Circulation for angle of attack 30

Figure 2.4. Variation of vortex circulation with the streamwise direction.

the circulation decreases as the vortex propagates downstream. This is because the vortex dissipates and loses energy as it is convected downstream and also due to its interaction with the boundary layer. In order to better observe the mean trends in the vortex circulation, the circulation values at all the streamwise cross-sections were averaged and plotted. Fig 2.5 shows this variation. It was also observed that the rate of vortex decay increases with angle of attack.

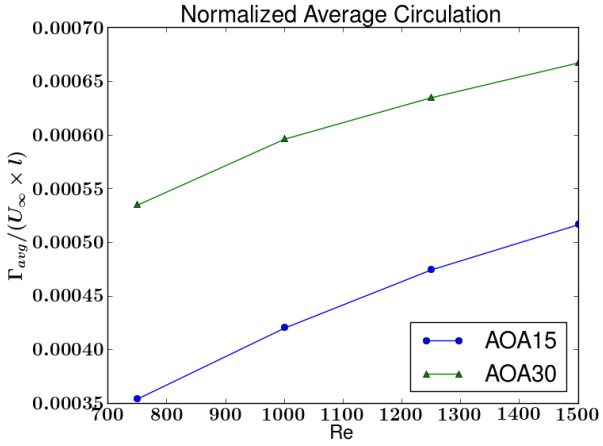

Figure 2.5. Average Circulation variation with Reynolds number and Angle of attack.

It can be seen from Fig 2.5 that the trends are similar to that of the average surface Nusselt number 2.3 and the average heat transfer enhancement varies exactly in the same way the circulation of the vortex does. The vortex is the driving mechanism of enhancement and this is the primary reason for the similar trends observed. Thus a higher value of circulation corresponds to an increased enhancement.

Similar to the findings of Marshall [14], a region of opposite sign streamwise vorticity was observed to be formed near the wall. Hence in order to quantify this opposite sign vorticity, similar analysis as above was done to find the boundary layer circulation or the streamwise vorticity content in the boundary layer. As a flat plate boundary layer has spanwise vorticity, the existence of streamwise content in the boundary layer could be attributed to the vortex-boundary layer interaction. Figure 2.6 shows the variation of the streamwise content of vorticity in the boundary layer.

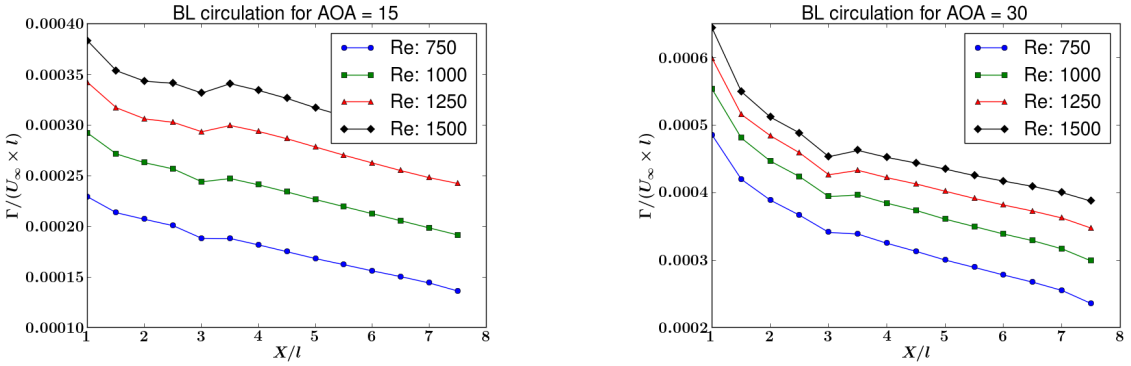

(a) Boundary layer circulation for angle of attack 15

(b) Boundary layer circulation for angle of attack 30

Figure 2.6. Variation of the streamwise content of vorticity in the boundary layer in the streamwise direction.

Similar to the vortex circulation, the boundary layer circulation was also observed to increase with increasing Reynolds number and angle of attack. It seemed to be dependent on the strength of the vortex being formed. However it can be seen

by comparing the slopes of figures 2.4 and 2.6 that the boundary layer circulation dissipates at a slower rate than the vortex.

A qualitative understanding of the vortex-boundary layer interaction can be visualized by isolating the vorticity around the vortex and the boundary layer. Fig. 2.7 shows isolated vorticity contours around the vortex while Fig. 2.8 shows isolated vorticity contours around the streamwise vorticity in the boundary layer.

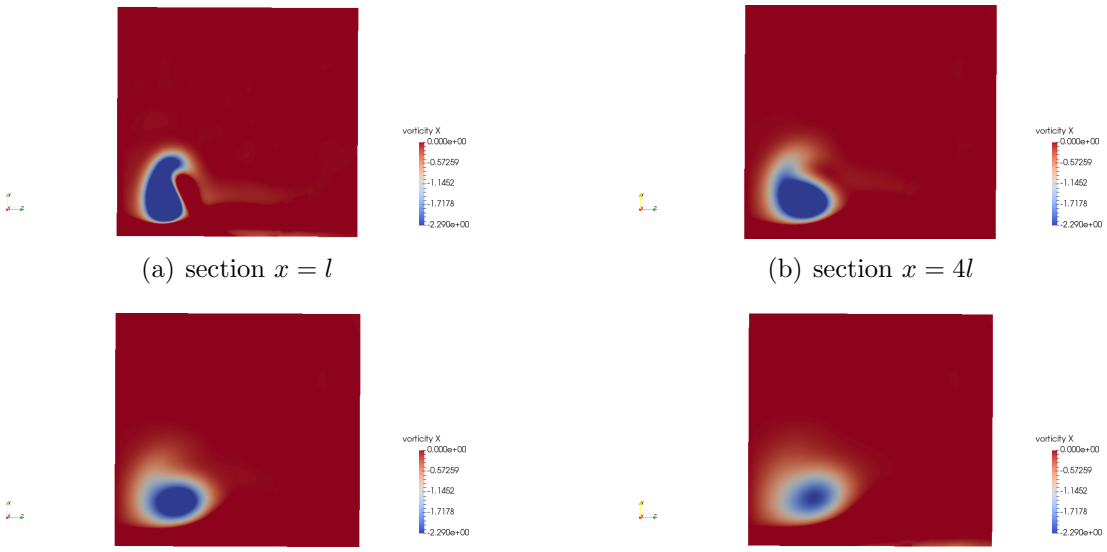

(a) section $x = l$ (b) section $x = 4l$

(c) section $x = 8l$ (d) section $x = 12l$

Figure 2.7. Isolated vorticity contours around the vortex at different spanwise sections.

It can be seen that the streamwise vorticity folds and wraps around the longitudinal vortex. This mechanism was also observed by Jimenez & Moin [13] in their DNS study of the near wall transition process in channel flows. They found this to be the instability causing mechanism. Thus the proximity of the vortex to the boundary layer redistributes the vorticity content within the boundary layer while the boundary layer acts as a dissipation mechanism to the longitudinal vortex.

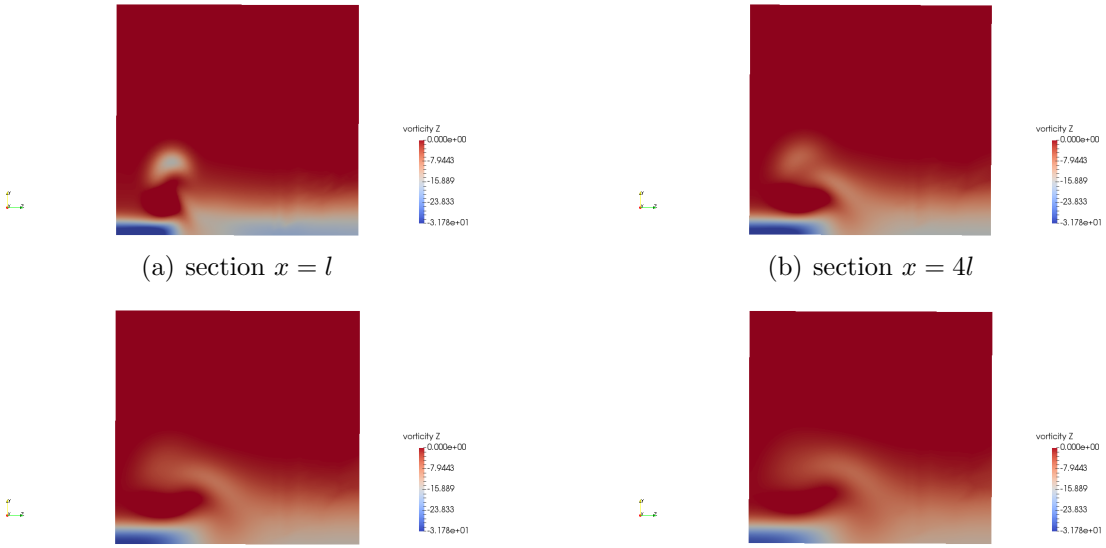

(a) section $x = l$ (b) section $x = 4l$

(c) section $x = 8l$ (d) section $x = 12l$

Figure 2.8. Isolated vorticity contours around the streamwise vorticity in the boundary layer at different spanwise sections.

Localized vorticity minimum was used to locate the vortex centers and the vortex trajectories were plotted. Figure 2.9 shows the position of the vortex centers for $\alpha = 15°$ and Fig. 2.10 for $\alpha = 30°$

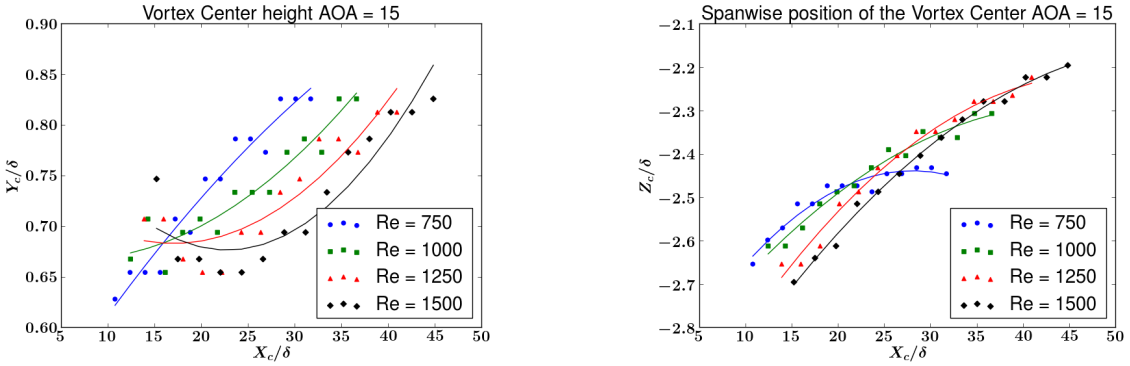

(a) Vortex center height (b) Spanwise position of the vortex center

Figure 2.9. Vortex center positions for $\alpha = 15°$.

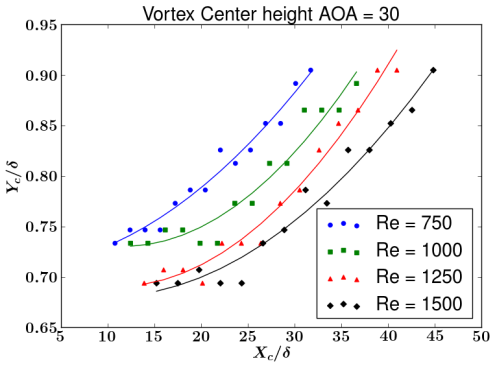

(a) Vortex center height

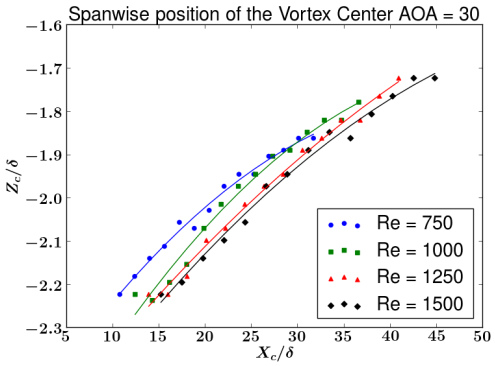

(b) Spanwise position of the vortex center

Figure 2.10. Vortex center positions for $\alpha = 30°$.

It is seen from Figures 2.9 and 2.10 that the vortex rises upwards as it is convected downstream. The reason for this being that the low pressure region inside the vortex generates an upwash from the wall and it rises as it propagates. The spanwise position seemed to be moving away from the center plane. This is due to the interaction of the vortex with its counter-rotational pair. As they have opposite sense of rotation, the flow in between the vortices pushes them apart slowly.

2.1.4 Validation of the use of slip boundary condition

In order to quantify the error in the assumption of the slip boundary condition imposed on the right wall of the domain, a study was performed. A configuration of Reynolds number 750 and $\alpha = 15°$ was chosen and an array of vortex generators side by side was considered. All the dimensions of the domain, the mesh and the methodology used for this case was kept the same as above. Figure 2.11 shows the domain and the mesh considered for this study.

The error in the assumption of the slip boundary condition can be gauged by observing the normal component of velocity at that surface as the slip condition

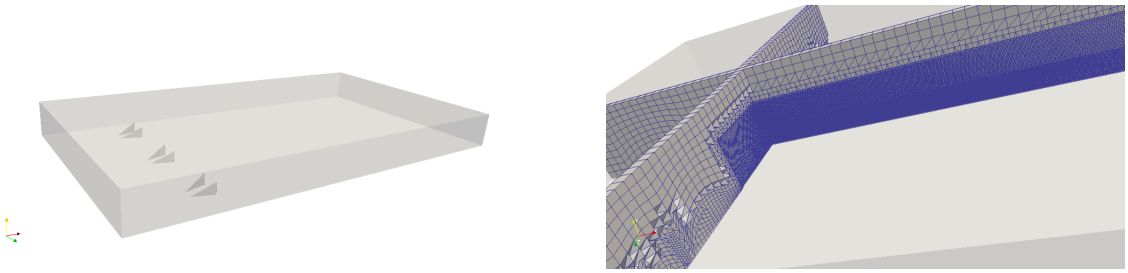

(a) Computational domain (b) Cross-sectional view of the mesh

Figure 2.11. Domain and mesh considered to validate the use of slip boundary condition.

enforces the normal component of velocity to be zero at the plane. Figure 2.12 shows the contour of the normal to the plane velocity component.

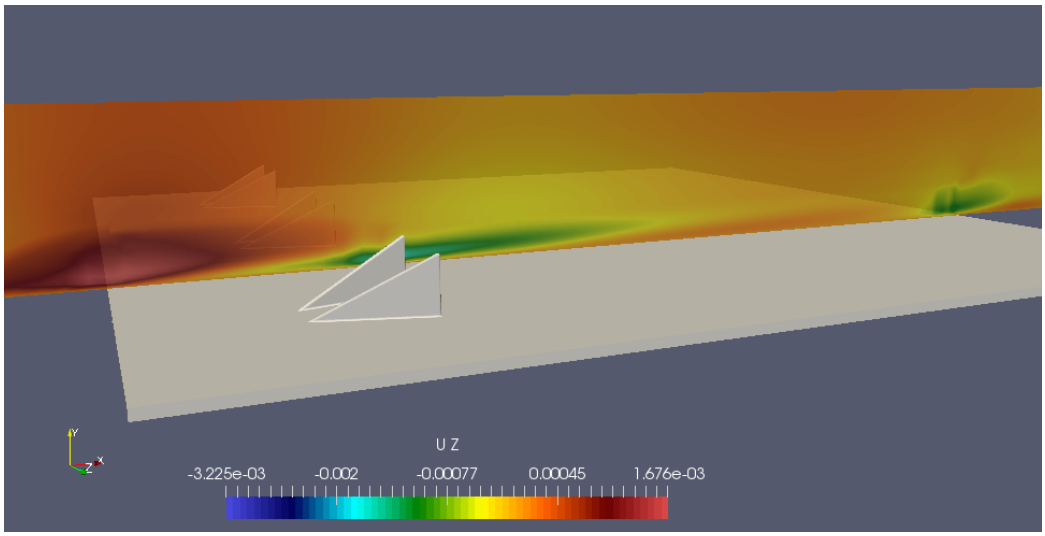

Figure 2.12. Contour of velocity component normal to the plane.

Figure 2.12 shows that the normal component of velocity is two orders of magnitude smaller than the tangential component. Thus there is little error in this assumption. Figure 2.13 shows the effect of this on the present calculations.

It is observed from Figure 2.13 that the boundary layer circulation does not change much and the maximum change in the vortex circulation is around 5%.

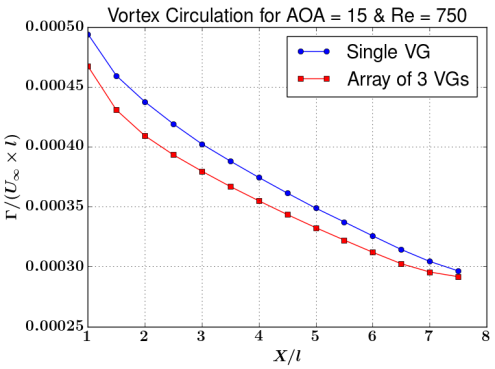

(a) Effect of slip condition on the Vortex circulation

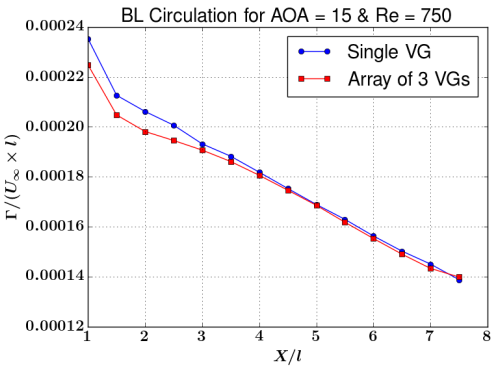

(b) Effect of slip condition on the Boundary layer circulation

Figure 2.13. Effect of slip wall boundary condition on the circulation.

CHAPTER 3

EFFECT OF BOUNDARY LAYER HEIGHT ON THE VORTEX CIRCULATION & HEAT TRANSFER

3.1 Methodology

Vortex generators can be classified as micro or macro vortex generators depending upon the height of the undisturbed boundary layer. If the height of the undisturbed boundary layer is higher than the vortex generator then that particular configuration is a micro vortex generator. And similarly if the height of the vortex generator is higher than the undisturbed boundary layer then the configuration is a macro vortex generator. Macro vortex generators are commonly used for heat transfer enhancements while micro vortex generators are commonly used for flow separation delay. All the previous cases were macro vortex generators and similar cases were run increasing the boundary layer height at the inlet. It was observed that the maximum undisturbed boundary layer height for all the previous cases was about $0.6\times$ the vortex generator height. In order to study the effect of boundary layer on the heat transfer enhancement and vortex circulation, micro vortex generator cases were studied. A custom boundary condition was implemented in OpenFOAM® to provide the laminar boundary layer profile. All the cells within the boundary layer were given a parabolic velocity profile and free-stream velocity was imposed for all the cells outside the boundary layer.

The maximum undisturbed boundary layer height was fixed to be $1.2 \times h$ where h is the vortex generator height and a parabolic velocity profile was given at the inlet such that the undisturbed boundary layer height is $1.2 \times h$. All previously run cases

were rerun using this changed inlet condition. All other boundary conditions and the solver settings were kept the same.

Figure 3.1 shows the inlet velocity contour and profile plotted on the center line.

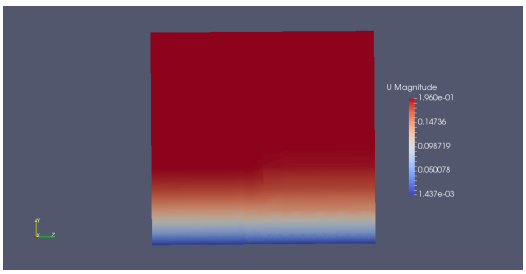

(a) Inlet velocity contour

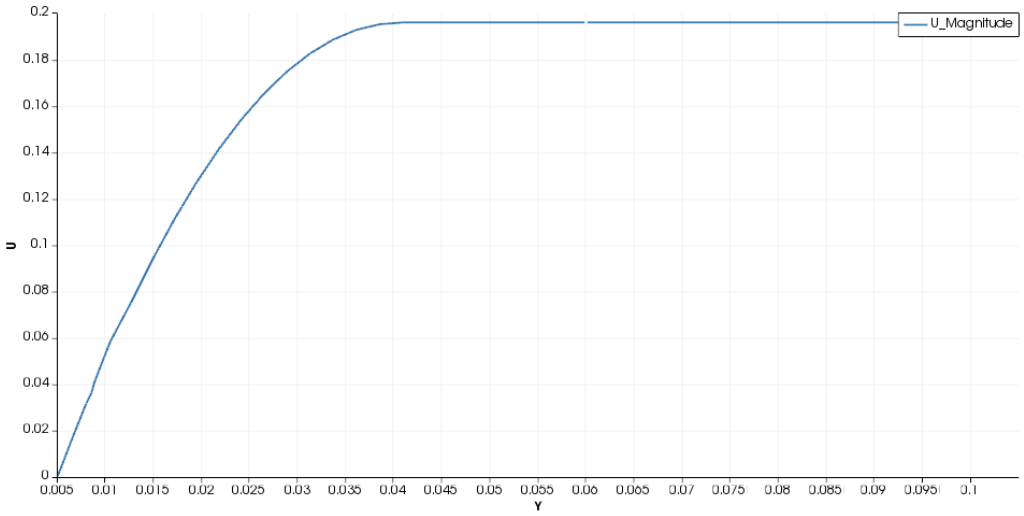

(b) Inlet velocity profile

Figure 3.1. Figure showing the inlet velocity contour and profile for the micro vortex generator cases.

As the vortex generator height is kept constant, the maximum undisturbed boundary layer height also remains the same for all the cases.

3.2 Results

The effect of boundary layer height on the heat transfer enhancement is important as it can help us understand which configuration is better suited for heat transfer enhancement if one provides better results than the other. Figure 3.2 shows the effect of increased boundary layer on the heat transfer enhancement.

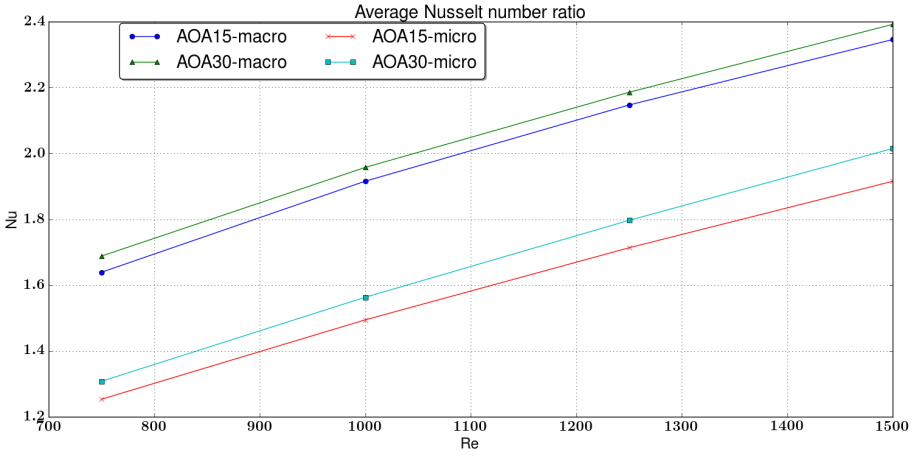

Figure 3.2. Average Nusselt number ratio variation.

As shown in figure 3.2, the trends seen in the heat transfer enhancement for the macro vortex generator case stays the same but the average enhancement is reduced. It can be said that the micro vortex generator is not as efficient for heat transfer enhancement as the macro vortex generator.

The logical explanation for this follows from the fact that the macro vortex generator sets up stirring scales outside of the boundary layer. Which is essential to entrain more colder flowing free-stream fluid over the plate. The stirring scales of the micro vortex generator is much closer to the wall and thus it is not able to entrain more of the free-stream fluid.

Similar trends were observed for the average circulation. Figure 3.3 shows a comparison of the average circulation for the macro and micro vortex generator cases.

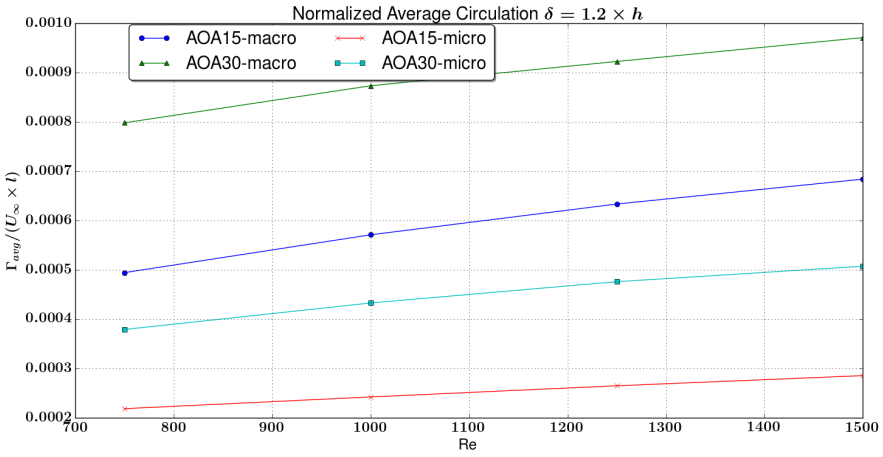

Figure 3.3. Average Circulation variation.

Thus a thicker boundary layer also reduces the average circulation of the vortex. This observation further bolsters the understanding that a higher value of circulation effectively signifies a higher heat transfer enhancement.

Figure 3.4 shows a comparison of the change in the streamwise variation of the circulation with the increase in the boundary layer height. It can be seen that as the ratio of the undisturbed boundary layer height to the vortex generator height (δ/h) is doubled, the vortex and the boundary layer circulation is almost reduced by half.

Figure 3.5 shows the streamwise variation of the vortex circulation with Reynolds number and angle of attack α , while Figure 3.6 shows the variation of the boundary layer circulation.

From Figure 3.5 it is seen that the vortex circulation decreases much more rapidly after a certain streamwise distance behind the vortex generator. This distance

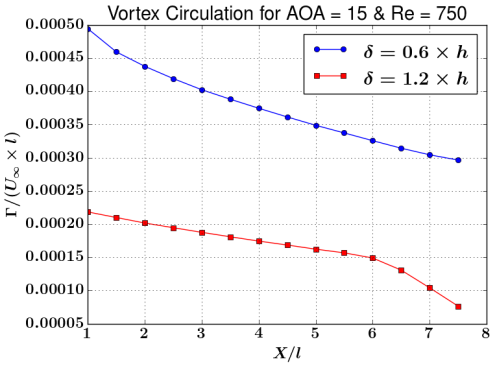

(a) Change in vortex circulation

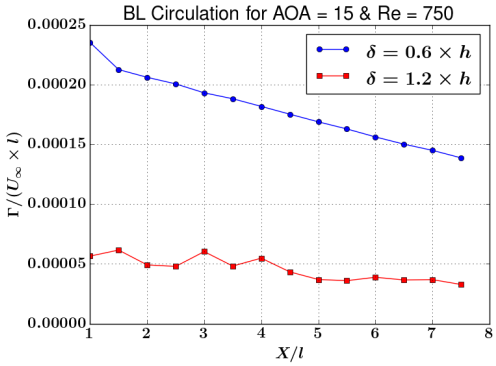

(b) Change in the boundary layer circulation

Figure 3.4. Comparison of the streamwise variation of the circulation.

was observed to be about $x = 6 \times l$ for $\alpha = 15°$ and $x = 6.5 \times l$ for $\alpha = 30°$, where l is the length of the vortex generator. It is also seen that this increased rate of decay also increases with Reynolds number. Thus at higher Reynolds number, the vortex decays faster after some distance behind the vortex generator. This increased decay coupled with reduced circulation of the vortex for the micro vortex generator is the reason for reduced heat transfer enhancement. The trends are similar to that observed in Figure 2.4. The vortex circulation increases with Reynolds number and α.

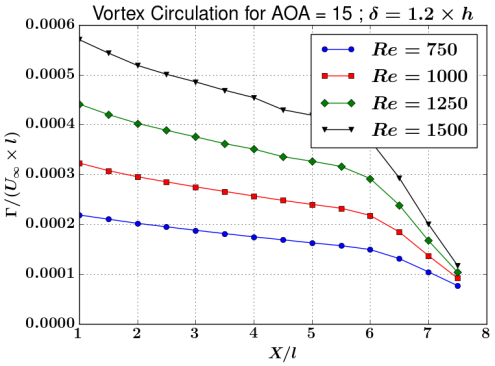

(a) Vortex circulation for $\alpha = 15°$

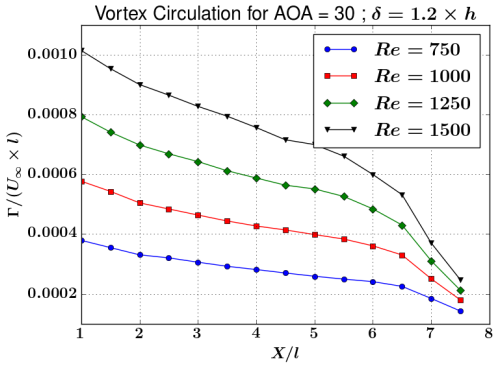

(b) Vortex circulation for $\alpha = 30°$

Figure 3.5. Streamwise variation of the vortex circulation for the micro vortex generator.

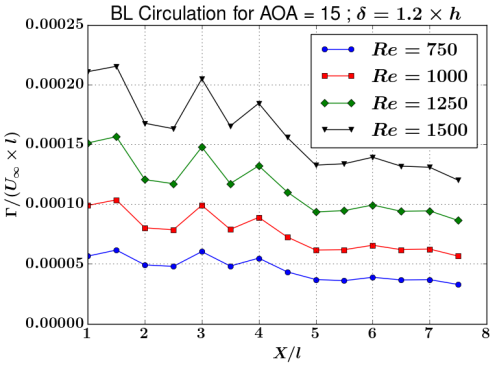

(a) Boundary layer circulation for $\alpha = 15°$

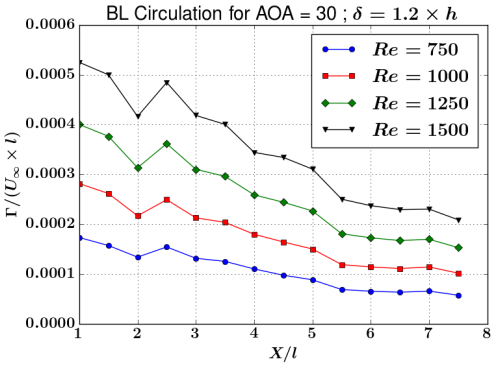

(b) Boundary layer circulation for $\alpha = 30°$

Figure 3.6. Streamwise variation of the boundary layer circulation for the micro vortex generator.

From Figure 3.6 it is seen that the streamwise vorticity content in the boundary layer decays much slower than that of the vortex. Beyond some streamwise distance it is observed that the boundary layer circulation does not change much. For the case of $\alpha = 15°$ this distance was observed to be equal to $5 \times l$ and $5.5 \times l$ for $\alpha = 30°$.

This suggests that beyond some distance, the streamwise content in the boundary layer is almost preserved while the circulation of the vortex decays rapidly when the boundary layer is thicker than the height of the vortex generator. The thicker boundary layer essentially changes the interaction of the vortex with the boundary layer and this has a direct influence on the overall heat transfer enhancement. In order to understand this change of interaction between the vortex and the boundary layer, it is important to identify the mechanisms that generate and destroy vorticity. Hence the vorticity transport equation was analyzed to identify the sources and sinks of vorticity. The following chapter describes the vorticity transport analysis.

CHAPTER 4

VORTICITY TRANSPORT

4.1 Derivation of the Vorticity Transport Equation

This section derives the integral form of the vorticity transport equation and gives the significance of the terms involved.

Shifting to a Lagrangian frame of reference that moves with the vortex, it is observed that the contour bounding the vortex also changes. The rate of change of circulation in this system is given by :-

$$\frac{d\Gamma}{dt} = \oint_{\partial A} \frac{\partial u}{\partial t}.ds \tag{4.1}$$

Following the work of Panah et al [34], substitution of the Navier-Stokes equations in equation 4.1 yields the following form

$$\frac{d\Gamma}{dt} = -\int_A [\nabla \times (\omega \times u)].n_A dA - \oint_{\partial A} \frac{dp}{\rho} - \oint_{\partial A} a_I.ds + \oint_{\partial A} \nu \nabla^2 u.ds \tag{4.2}$$

Where n_A is the unit surface normal to the streamwise direction, a_I is the local acceleration of the inertial reference frame which is zero for this study. The pressure integral vanishes for incompressible flow since the density is constant. Since all the results gathered for the micro and macro vortex generator cases so far are steady state, a change of variable is applied to the rate of change of circulation as follows:-

$$\frac{d\Gamma}{dt} = \frac{dx}{dt}.\frac{d\Gamma}{dx} \tag{4.3}$$

i.e

$$\frac{d\Gamma}{dt} = u_x.\frac{d\Gamma}{dx} \tag{4.4}$$

Thus equation 4.2 reduces to

$$u_x.\frac{d\Gamma}{dx} = -\int_A [\nabla \times (\omega \times u)].n_A dA + \oint_{\partial A} \nu.\nabla^2 u.ds \tag{4.5}$$

The first term on the right hand side expands to

$$-\int_A [\nabla \times (\omega \times u)].n_A dA = -\int_A [\frac{\partial(u_y\omega_x)}{\partial y} - \frac{\partial(u_x\omega_y)}{\partial y} - \frac{\partial(u_x\omega_z)}{\partial z} + \frac{\partial(u_z\omega_x)}{\partial z}]dA \tag{4.6}$$

Using the chain rule, to expand the terms

$$\begin{aligned}-\int_A [\nabla \times (\omega \times u)].n_A dA = -\int_A [u_y\frac{\partial\omega_x}{\partial y} + \omega_x\frac{\partial u_y}{\partial y} - u_x\frac{\partial\omega_y}{\partial y} - \omega_y\frac{\partial u_x}{\partial y} - u_x\frac{\partial\omega_z}{\partial z} \\ - \omega_z\frac{\partial u_x}{\partial z} + u_z\frac{\partial\omega_x}{\partial z} + \omega_x\frac{\partial u_z}{\partial z}]dA\end{aligned} \tag{4.7}$$

Rearranging the terms and simplifying,

$$\begin{aligned}-\int_A [\nabla \times (\omega \times u)].n_A dA = -\int_A [-u_x(\frac{\partial\omega_y}{\partial y} + \frac{\partial\omega_z}{\partial z}) - (\omega_y\frac{\partial u_x}{\partial y} + \omega_z\frac{\partial u_x}{\partial z}) + (u_y\frac{\partial\omega_x}{\partial y} \\ + u_z\frac{\partial\omega_x}{\partial z}) + \omega_x(\frac{\partial u_y}{\partial y} + \frac{\partial u_z}{\partial z})]dA\end{aligned} \tag{4.8}$$

The vector calculus identity $\nabla.(\nabla \times u) = 0$ and the incompressibility condition $\nabla.u = 0$ are used to simplify equation 4.8. i.e.

$$\nabla.(\nabla \times u) = \frac{\partial\omega_x}{\partial x} + \frac{\partial\omega_y}{\partial y} + \frac{\partial\omega_z}{\partial z} = 0 \implies \frac{\partial\omega_y}{\partial y} + \frac{\partial\omega_z}{\partial z} = -\frac{\partial\omega_x}{\partial x} \tag{4.9}$$

$$\nabla.u = \frac{\partial u_x}{\partial x} + \frac{\partial u_y}{\partial y} + \frac{\partial u_z}{\partial z} = 0 \implies \frac{\partial u_y}{\partial y} + \frac{\partial u_z}{\partial z} = -\frac{\partial u_x}{\partial x} \tag{4.10}$$

Substituting these in equation 4.8;

$$-\int_A [\nabla \times (\omega \times u)].n_A dA = \int_A [-u_x \frac{\partial \omega_x}{\partial x} + (\omega_y \frac{\partial u_x}{\partial y} + \omega_z \frac{\partial u_x}{\partial z}) + (u_y \frac{\partial \omega_x}{\partial y} + u_z \frac{\partial \omega_x}{\partial z}) - \omega_x \frac{\partial u_x}{\partial x}] dA \quad (4.11)$$

The diffusion term can be written as an area integral applying the Stoke's theorem

$$\oint_{\partial A} \nu \nabla^2 u.ds = \int_A \nu (\frac{\partial^2 \omega_x}{\partial x^2} + \frac{\partial^2 \omega_y}{\partial y^2} + \frac{\partial^2 \omega_z}{\partial z^2}) dA$$

Thus equation 4.2 becomes,

$$u_x \frac{d\Gamma}{dx} + \int_A u_x \frac{\partial \omega_x}{\partial x} dA - \int_A \omega_y \frac{\partial u_x}{\partial y} dA - \int_A \omega_z \frac{\partial u_x}{\partial z} dA + \int_A \omega_x \frac{\partial u_x}{\partial x} dA - \int_A u_y \frac{\partial \omega_x}{\partial y} dA - \int_A u_z \frac{\partial \omega_x}{\partial z} - \int_A \nu (\frac{\partial^2 \omega_x}{\partial x^2} + \frac{\partial^2 \omega_y}{\partial y^2} + \frac{\partial^2 \omega_z}{\partial z^2}) dA + \Phi = 0 \quad (4.12)$$

Equation 4.12 is the vorticity transport equation.

- $u_x \frac{d\Gamma}{dx}$ is the rate of change of circulation.
- $\int_A u_x \frac{\partial \omega_x}{\partial x} dA$ is the flux of vorticity due to the streamwise convection of the vortex.
- $\int_A \omega_y \frac{\partial u_x}{\partial y} dA$ term denotes the flux of vorticity due to tilting in the Y direction.
- $\int_A \omega_z \frac{\partial u_x}{\partial z} dA$ is the flux of vorticity due to tilting in the z direction (spanwise direction).
- $\int_A (u_y \frac{\partial \omega_x}{\partial y} + u_z \frac{\partial \omega_x}{\partial z}) dA - \int_A \omega_x \frac{\partial u_x}{\partial x} dA$ is the flux associated with the shear layer.
- $\int_A \nu (\frac{\partial^2 \omega_x}{\partial x^2} + \frac{\partial^2 \omega_y}{\partial y^2} + \frac{\partial^2 \omega_z}{\partial z^2}) dA$ is the flux associated with the diffusion of the vortex.
- Φ represents the annihilation of vorticity due to entrainment and interaction with the streamwise content of vorticity in the boundary layer.

In the current study the Φ term is inferred from the analysis of other terms, as in the work of Wojcik [35]. In this work, Φ is defined as positive when it results in the annihilation of negative vorticity and negative when it results in the annihilation of positive vorticity. For all the cases, the vortex has negative vorticity and the boundary layer has positive streamwise vorticity. Thus it is expected to have a positive Φ for the vortex and negative Φ for the streamwise content of vorticity in the boundary layer.

4.2 Methodology

All the results of the vorticity transport analysis were calculated in the post-processing step. An application was written in C++ using the classes and methods available in OpenFOAM®. This application reads the velocity field, computes the vorticity field and then evaluates all the terms of equation 4.12 within the area integral. Using OpenFOAM's library has many advantages like the availability of well tested and verified second order methods to evaluate the derivatives and parallelization of the calculations.

All the above mentioned derivatives in the vorticity transport equation were calculated using second order schemes for the entire domain and written as field values at the cell centers. Thus all the terms within the area integrals were available to be extracted on to the spanwise sections. And according to the previously defined contours, the area integrals were calculated for each spanwise section and plotted. As the vortex and boundary layer circulation data is already known from the previous analysis, the rate of change of circulation was calculated using a centered difference scheme. All the terms were then non-dimensionalized with U_∞^2.

The analysis was performed for all the cases previously run for micro and macro vortex generators. The goal of this study was to gauge the reason for the change in

interaction of the vortex and the boundary layer between the micro and macro vortex generator cases. The results are compared in the next section.

4.3 Results & Discussion

Vorticity budget for all the cases is presented here. It was observed that the contribution of the tilting and diffusion fluxes were negligible. Shear, convection and the interaction terms were the dominant mechanisms of vorticity transport.

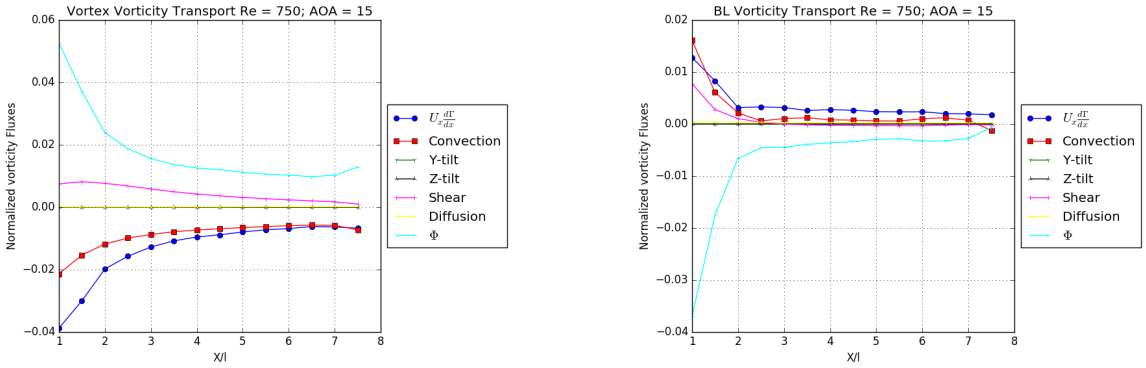

(a) vortex vorticity transport $Re = 750; \alpha = 15°$

(b) boundary layer vorticity transport $Re = 750; \alpha = 15°$

Figure 4.1. Figure showing the vorticity fluxes of the macro vortex generators for $Re = 750; \alpha = 15°$.

Figure 4.1 shows that the rate of change of circulation decreases gradually in the streamwise direction while that of the boundary layer more or less stays constant after some distance in the streamwise direction. It can also be observed that the shear flux for the boundary layer vorticity budget, decreases rapidly and is negligible after some distance in the streamwise direction. This suggests that for the boundary layer circulation, the convection flux is more dominant and the boundary layer circulation decays due to the action of convection and interaction with the vortex. The interaction

term Φ has opposite signs for the vortex and the boundary layer vorticity. This is because the vortex and the streamwise vorticity in the boundary layer have opposing signs.

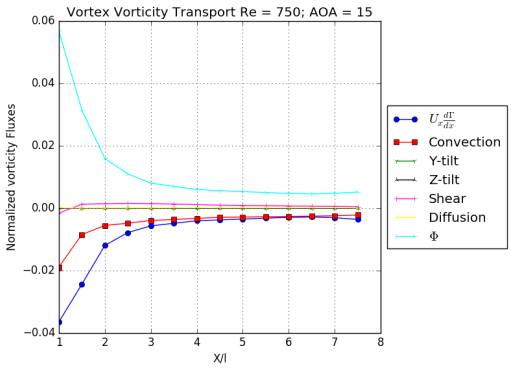

(a) vortex vorticity transport $Re = 750; \alpha = 15°$

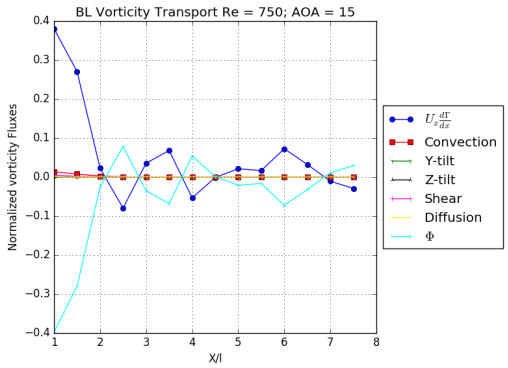

(b) boundary layer vorticity transport $Re = 750; \alpha = 15°$

Figure 4.2. Figure showing the vorticity fluxes of the micro vortex generators for $Re = 750; \alpha = 15°$.

Comparing Figures 4.1 and 4.2 it can be seen that for the micro vortex generator, the shear flux is negligible compared to the macro vortex generator. The interaction term and the rate of change of vortex circulation have similar trends. The boundary layer vorticity fluxes change considerably for the case of the micro vortex generators. It was observed that the rate of change of circulation and the interaction term fluctuate between positive and negative. This suggests that there is both creation and destruction of streamwise vorticity in the boundary layer. Since only the streamwise transport of vorticity is analyzed, it is difficult to interpret this behaviour. A possible reason of this might be due to the fact that a thicker boundary layer has more spanwise vorticity and there might be some conversion of the spanwise vorticity in to the streamwise component.

This alternating generation and destruction of streamwise boundary layer vorticity however vanishes with increased angle of attack as can be seen from Figs 4.10 to 4.16. This is attributed to the fact that an increase in α also increases the vortex and the boundary layer circulation and it is less sensitive to the fluxes.

Another observation that can be made from this study is that the vorticity fluxes for the macro vortex generator cases are around the same order of magnitude. The magnitude of the rate of change of the boundary layer circulation and the interaction term Φ for the transport of boundary layer vorticity increases with increasing Reynolds number and angle of attack.

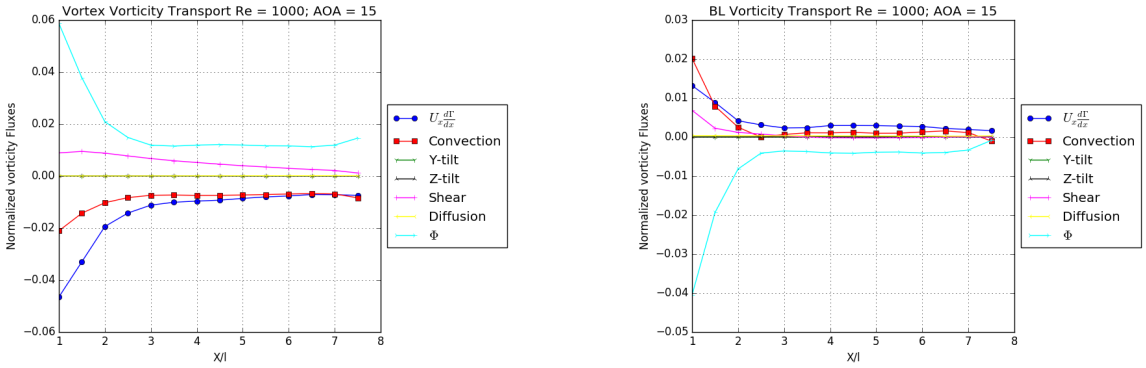

(a) vortex vorticity transport $Re = 1000; \alpha = 15°$

(b) boundary layer vorticity transport $Re = 1000; \alpha = 15°$

Figure 4.3. Figure showing the vorticity fluxes of the macro vortex generators for $Re = 1000; \alpha = 15°$.

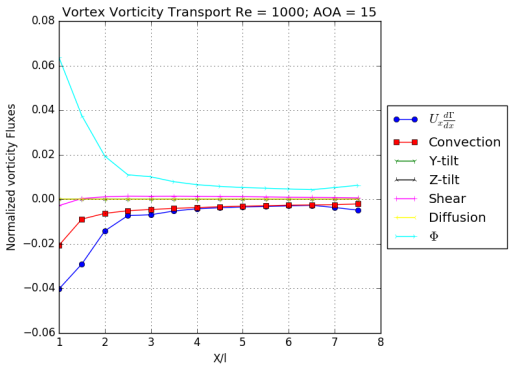

(a) vortex vorticity transport $Re = 1000; \alpha = 15°$

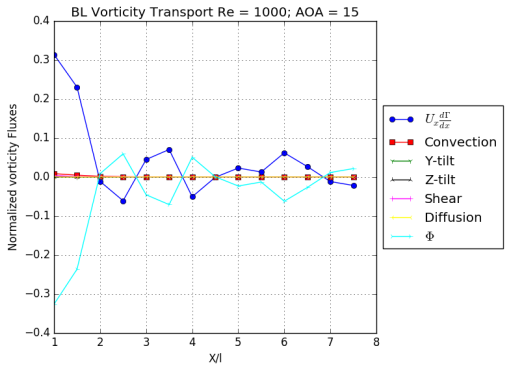

(b) boundary layer vorticity transport $Re = 1000; \alpha = 15°$

Figure 4.4. Figure showing the vorticity fluxes of the micro vortex generators for $Re = 1000; \alpha = 15°$.

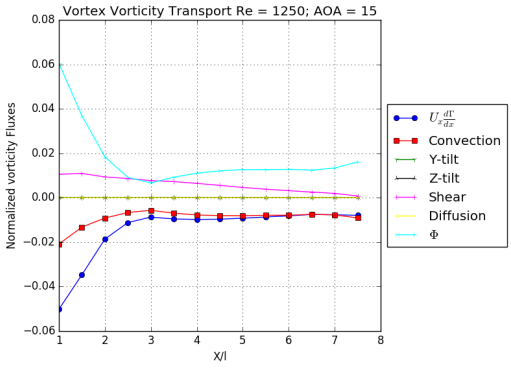

(a) vortex vorticity transport $Re = 1250; \alpha = 15°$

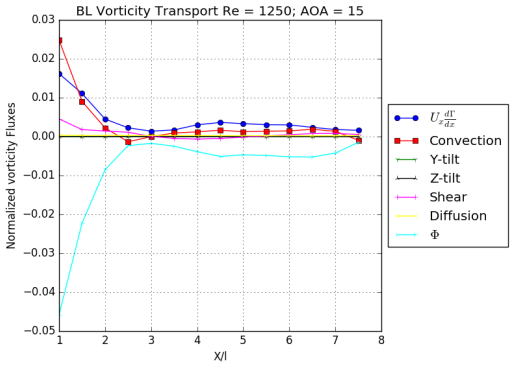

(b) boundary layer vorticity transport $Re = 1250; \alpha = 15°$

Figure 4.5. Figure showing the vorticity fluxes of the macro vortex generators for $Re = 1250; \alpha = 15°$.

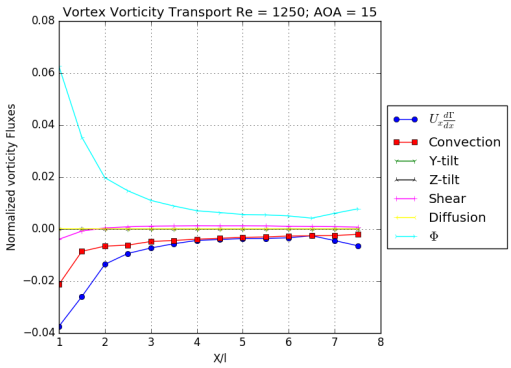

(a) vortex vorticity transport $Re = 1250; \alpha = 15°$

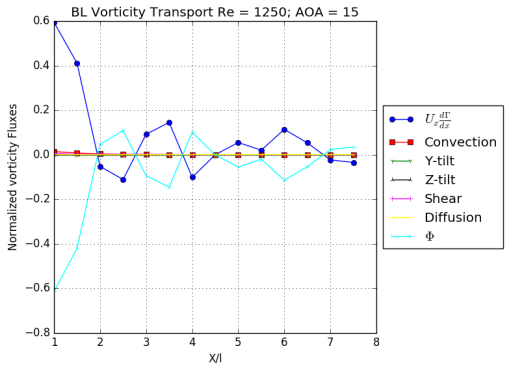

(b) boundary layer vorticity transport $Re = 1250; \alpha = 15°$

Figure 4.6. Figure showing the vorticity fluxes of the micro vortex generators for $Re = 1250; \alpha = 15°$.

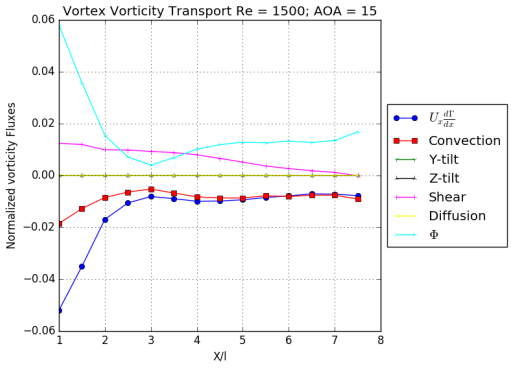

(a) vortex vorticity transport $Re = 1500; \alpha = 15°$

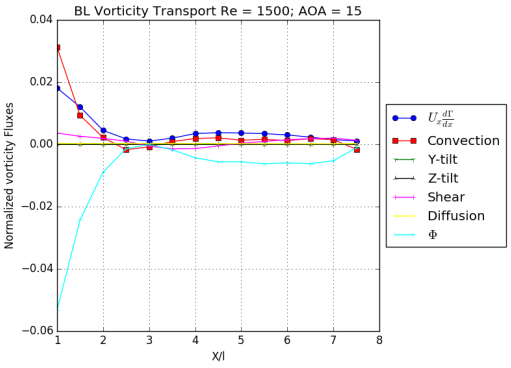

(b) boundary layer vorticity transport $Re = 1500; \alpha = 15°$

Figure 4.7. Figure showing the vorticity fluxes of the macro vortex generators for $Re = 1500; \alpha = 15°$.

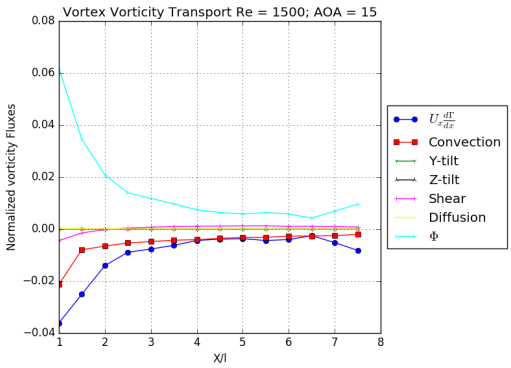

(a) vortex vorticity transport $Re = 1500; \alpha = 15°$

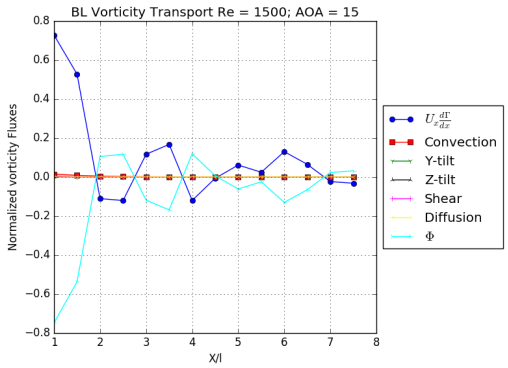

(b) boundary layer vorticity transport $Re = 1500; \alpha = 15°$

Figure 4.8. Figure showing the vorticity fluxes of the micro vortex generators for $Re = 1500; \alpha = 15°$.

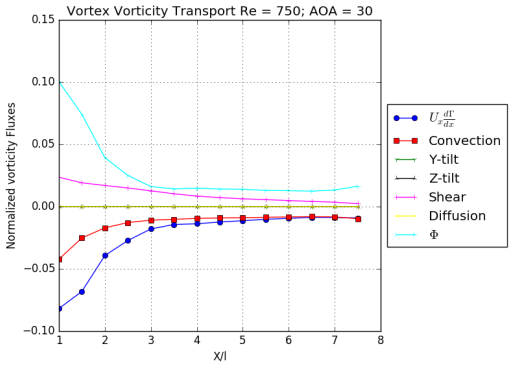

(a) vortex vorticity transport $Re = 750; \alpha = 30°$

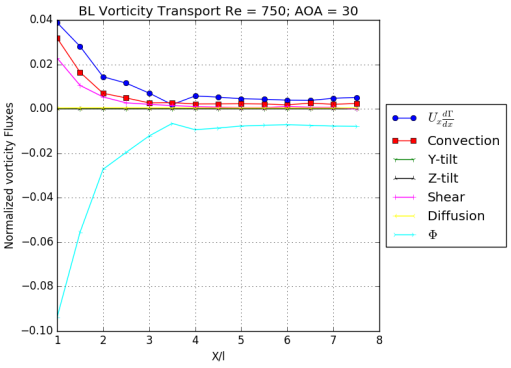

(b) boundary layer vorticity transport $Re = 750; \alpha = 30°$

Figure 4.9. Figure showing the vorticity fluxes of the macro vortex generators for $Re = 750; \alpha = 30°$.

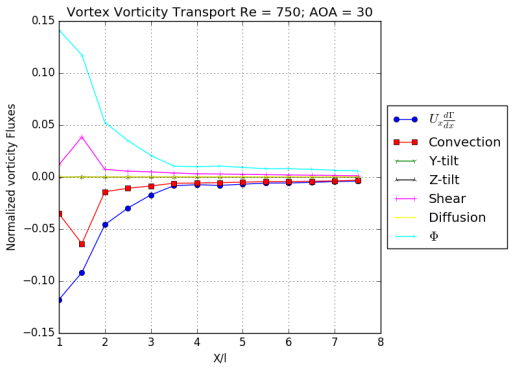

(a) vortex vorticity transport $Re = 750; \alpha = 30°$

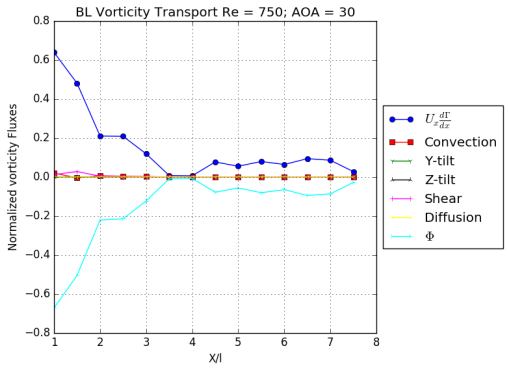

(b) boundary layer vorticity transport $Re = 750; \alpha = 30°$

Figure 4.10. Figure showing the vorticity fluxes of the micro vortex generators for $Re = 750; \alpha = 30°$.

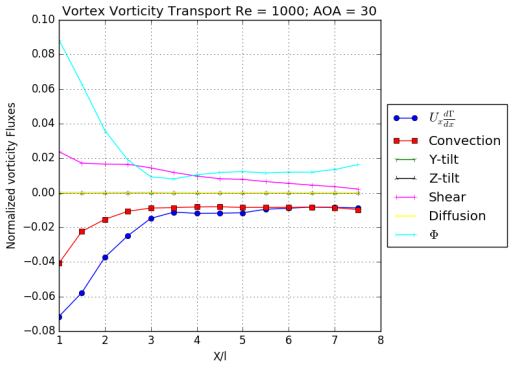

(a) vortex vorticity transport $Re = 1000; \alpha = 30°$

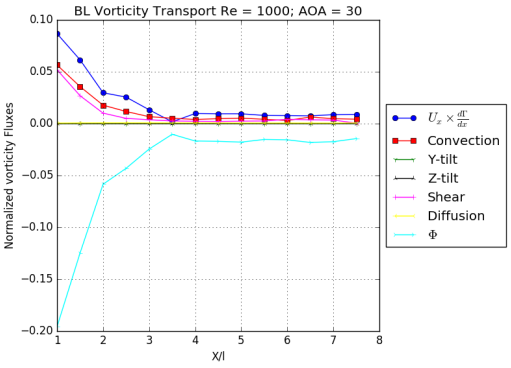

(b) boundary layer vorticity transport $Re = 1000; \alpha = 30°$

Figure 4.11. Figure showing the vorticity fluxes of the macro vortex generators for $Re = 1000; \alpha = 30°$.

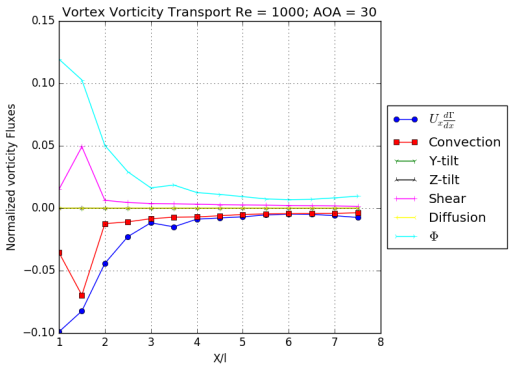

(a) vortex vorticity transport $Re = 1000; \alpha = 30°$

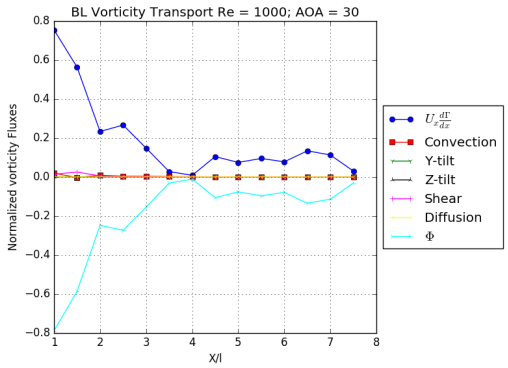

(b) boundary layer vorticity transport $Re = 1000; \alpha = 30°$

Figure 4.12. Figure showing the vorticity fluxes of the micro vortex generators for $Re = 1000; \alpha = 30°$.

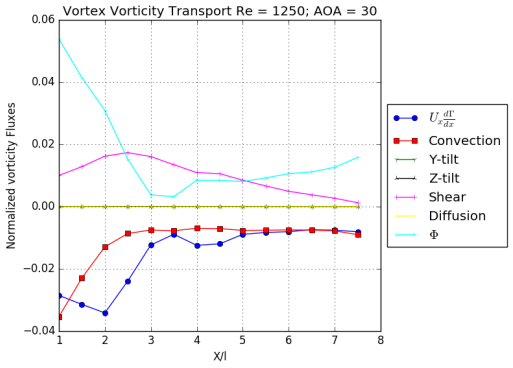

(a) vortex vorticity transport $Re = 1250; \alpha = 30°$

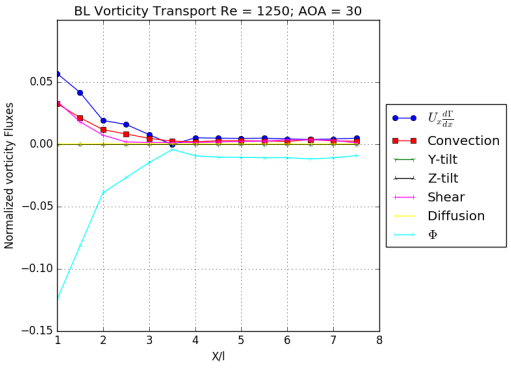

(b) boundary layer vorticity transport $Re = 1250; \alpha = 30°$

Figure 4.13. Figure showing the vorticity fluxes of the macro vortex generators for $Re = 1250; \alpha = 30°$.

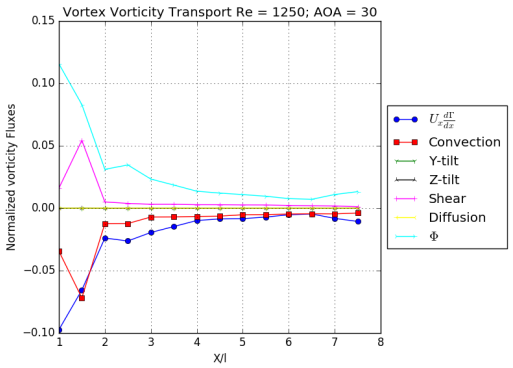

(a) vortex vorticity transport $Re = 1250; \alpha = 30°$

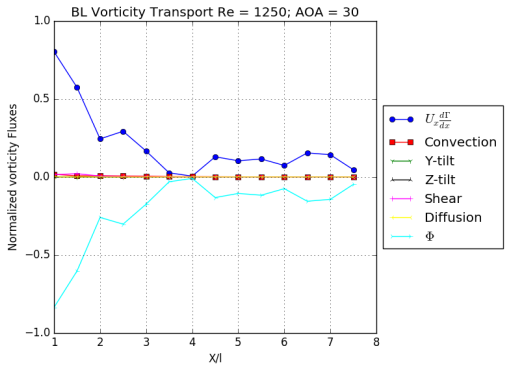

(b) boundary layer vorticity transport $Re = 1250; \alpha = 15°$

Figure 4.14. Figure showing the vorticity fluxes of the micro vortex generators for $Re = 1250; \alpha = 30°$.

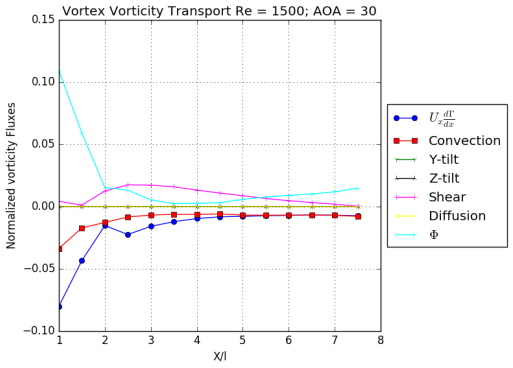

(a) vortex vorticity transport $Re = 1500; \alpha = 30°$

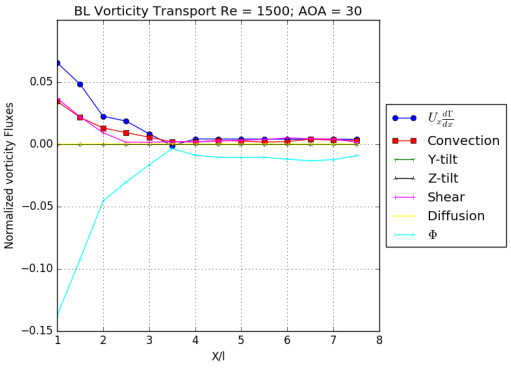

(b) boundary layer vorticity transport $Re = 1500; \alpha = 30°$

Figure 4.15. Figure showing the vorticity fluxes of the macro vortex generators for $Re = 1500; \alpha = 30°$.

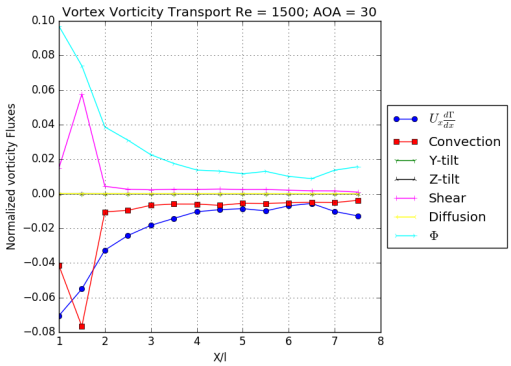

(a) vortex vorticity transport $Re = 1500; \alpha = 30°$

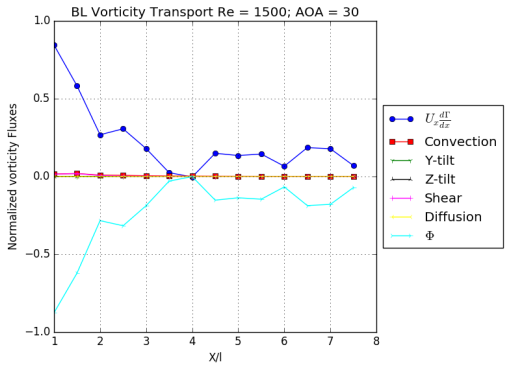

(b) boundary layer vorticity transport $Re = 1500; \alpha = 30°$

Figure 4.16. Figure showing the vorticity fluxes of the micro vortex generators for $Re = 1500; \alpha = 30°$.

CHAPTER 5

INFLUENCE OF SHEDDING ON HEAT TRANSFER ENHANCEMENT

It was observed for the case of $\alpha = 45^\circ$ that vortices are shed periodically from the vortex generator. The influence of shedding on heat transfer enhancement is important for design considerations. If the average heat transfer enhancement increases considerably because of shedding then optimal design of vortex generators should instigate this.

Due to the shedding, the assumption of symmetric flow field might be invalid. Hence for this case, the entire domain was considered. Figure 5.1 shows a time instant of the $\lambda 2$ criterion (Jeong & Hussain [36]) isocontour to visualize the shedding characteristics. $\lambda 2$ refers to the second eigenvalue of the velocity gradient tensor. It is widely used to visualize coherent structures as $\lambda 2 < 0$ isolates a region of local pressure minimum.

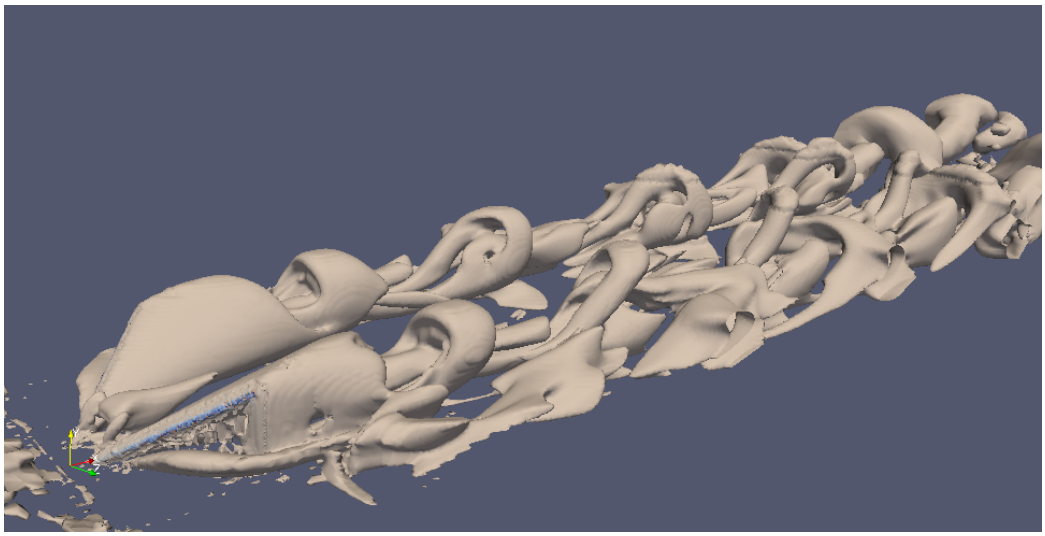

Figure 5.1. $\lambda 2$ criterion isocontour plotted to visualize the vortex shedding.

Figure 5.1 shows that the shedding of vortices is complex and three dimensional. Hairpin like structures can be seen convecting downstream.

5.1 Computational Domain and Mesh

Figure 5.2 shows the computational domain modeled and the mesh used for this case.

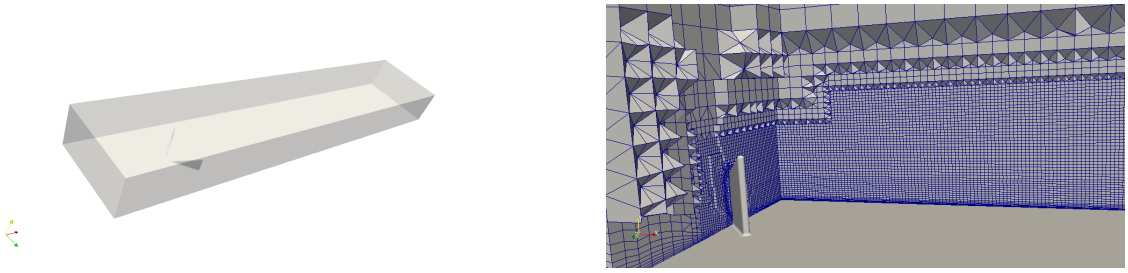

(a) Computational domain (b) Mesh around the vortex generator

Figure 5.2. Computational domain and mesh used for the case of $\alpha = 45°$.

Similar to all the previous cases, this mesh was also generated in OpenFOAM® consisting of around 4.5 million cells. The cells were refined around the vortex generator and in the wake region. Figure 5.2 shows a zoomed in view of the mesh around the vortex generator.

Second order implicit Crank-Nicholson scheme was used for the temporal discretization. 8 probes were placed at different locations in the vortex generator wake to collect temporal data for the calculation of shedding frequency and Strouhal number. The simulations were run until a steady state amplitude of the temporal fluctuations were observed. Figure 5.3 shows the steady state amplitude along with the Fast Fourier Transform of the probe data.

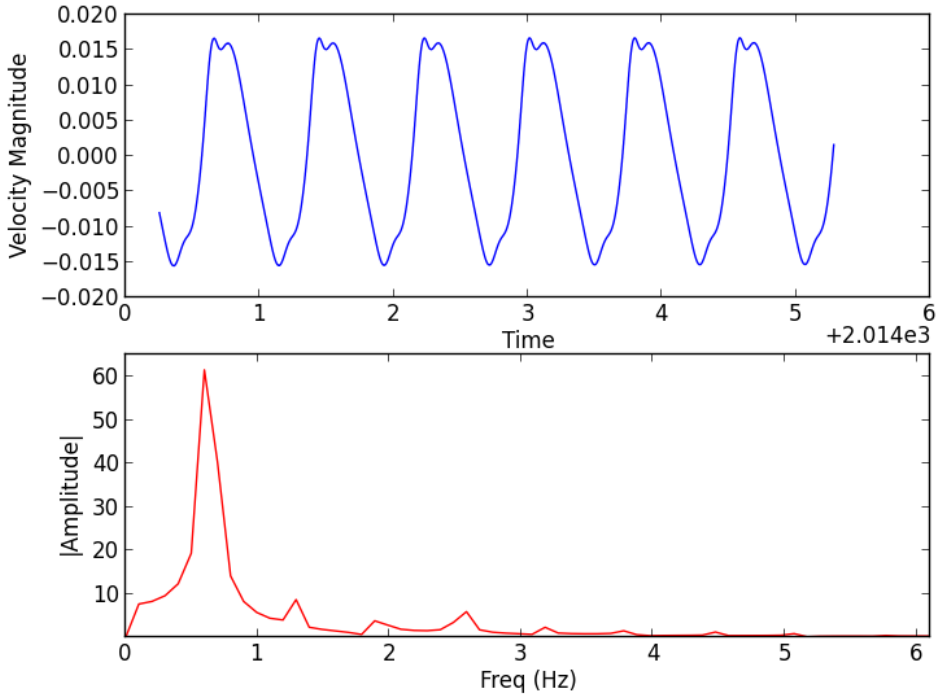

Figure 5.3. Probe data taken for the case of $Re = 750; \alpha = 45°$.

The frequencies calculated in this manner was used to calculate the flow Strouhal number which is a non-dimensional parameter used to describe frequency. The Strouhal number was calculated based on the free-stream velocity U_∞ and the vortex generator length l.

$$St = fl/U_\infty \tag{5.1}$$

Where f is the vortex shedding frequency.

5.2 Reynolds - Strouhal Number Relationship

Figure 5.4 shows a plot of Strouhal number vs Reynolds number. Results were obtained for cases $Re = 750 - 1500$. From figure 5.4. The Strouhal number for the

range of Reynolds number considered lies within 0.2 to 0.3. This trend is similar to the trend observed for the cylinder wakes, which suggests that the instability causing the shedding might be a bluff body instability. As the angle of attack of the vortex generator is increased, the frontal obstruction to the flow increases and the vortex generator resembles a bluff body.

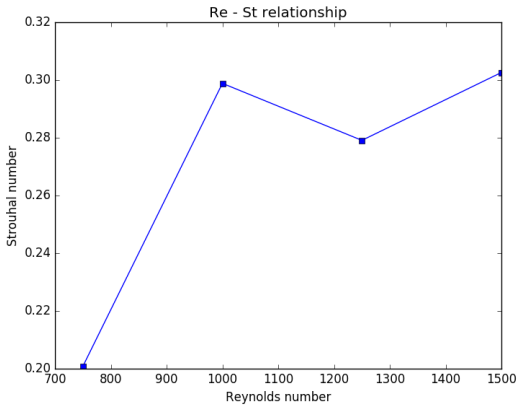

Figure 5.4. Figure showing the Reynolds number and Strouhal number relationship.

5.3 Effects on Heat Transfer

All the cases were time averaged over a cycle after ensuring that the amplitude of the oscillations stays the same with time. Time averaged quantities were used to calculate the average heat transfer enhancement following the procedure outlined in Chapter 2

Figure 5.5 shows the comprehensive comparison of the heat transfer enhancement of all the cases so far. It can be seen that the shedding reduces the average heat transfer enhancement. Fiebig [10] observed in his studies that the enhancement increases up to a maximum limit with angle of attack and then decreases above some angle. This might be attributed to the unsteady shedding observed in the current

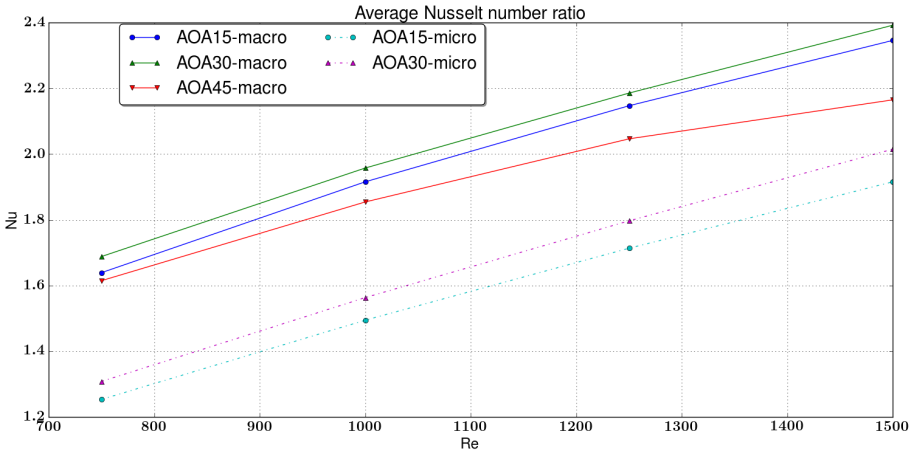

Figure 5.5. Figure showing the heat transfer enhancement comparisons for all the cases.

study. The shedding of vortices is not effective to entrain the free-stream fluid over the heated surface and hence a lower overall enhancement is observed for this case. The enhancement increases with increasing vortex circulation as a stronger vortex entrains more free-stream fluid. Thus in order to maximize the heat transfer, vortex shedding should be inhibited. Camarri & Lollo [37] designed a feedback control to suppress the vortex shedding behind a square cylinder in a channel flow by actuating two jets on the cylinder surface. It would be interesting to design a similar mechanism to inhibit the shedding for the case of $\alpha = 45^{\circ}$ and observe the heat transfer characteristics.

The only drawback of using vortex generators is that they result in additional frictional losses. Thus the skin friction coefficient was calculated for all the cases. This was then normalized with the baseline case of the flat plate using the correlations available. Proper care was taken in using the length of the flat plate for the baseline calculations such that it is representative of the respective cases and time averaged velocity was used to calculate the skin friction coefficient for the case of $\alpha = 45^{\circ}$.

The thermal performance parameter was then calculated using the Nusselt number ratio Nu and the skin friction coefficient ratio C_f as Sheikholeslami et al. [38] defined:-

$$T.P.P. = \frac{Nu}{C_f^{1/3}} \tag{5.2}$$

The thermal performance parameter is indicative of the cumulative effect of enhancement along with a penalty imposed for increasing the frictional losses. Figure 5.6 shows the observed trends.

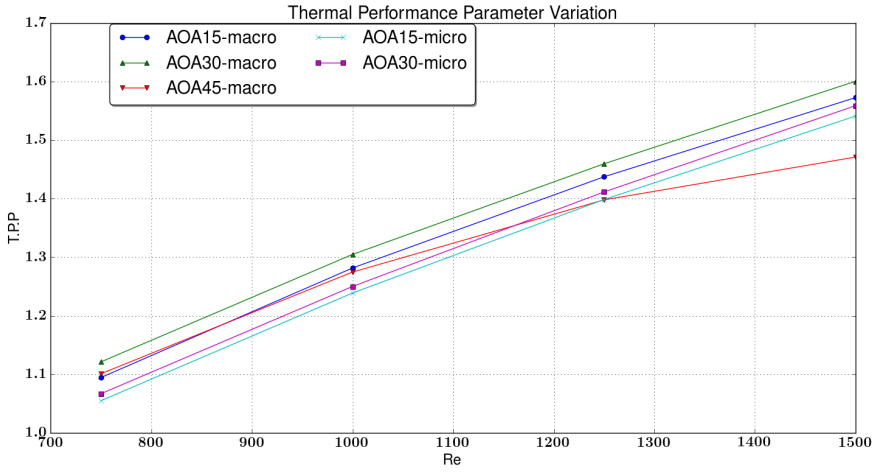

Figure 5.6. Figure showing the thermal performance parameter trend comparison for all the cases.

It was observed from Figure 5.6 that the thermal performance parameter for the case of $\alpha = 30°$ was the maximum. Lower C_f values for the micro vortex generator cases were observed which explains the upward shift in plot as compared to Figure 5.5. Thus it is conclusively observed that the overall thermal performance of the macro vortex generators is better than that of the micro vortex generators.

CHAPTER 6

VORTEX GENERATOR WITH JET IN CROSS-FLOW

In this Chapter the effect of vortex generator on the mixing characteristics of the jet in cross-flow is studied. Two different configurations of the vortex generators namely Flow-Up and Flow-Down configurations shown in Fig. 1.1 were studied to compare their results. The motivation for considering the Flow-Up configuration comes from Wang et al. [28] where they observed that the performance of these two configurations were not alike for heat impingement heat transfer. They observed that the Flow-Up configuration provided better results and increased the jet penetration depth. The goal of this study is to check if a similar trend can be observed for the mixing enhancement. The velocity ratio i.e. the ratio of the velocity of the jet to the velocity of the cross-stream was taken to be equal to 2.5.

The first half of the Chapter shows the validation case considered for the study of the jet in cross-flow.

6.1 Preliminary Study of the Jet in Cross-flow

6.1.1 Computational domain & Mesh

The computational domain considered in this study was taken to be of the same dimensions as in Muppidi & Mahesh [2] as they had studied the confinement effects on the jet and noted that a domain of $32d \times 64d \times 64d$ does not constrain the jet. Here d is the diameter of the jet orifice. The mesh was generated in OpenFOAM®. Prismatic cells were added for accurately resolving the boundary layer. The mesh consisted of about 10 million cells. According to the extents of the jet in the domain

as specified in [2], the interior region was refined. Figure 6.1 shows the mesh used in this study.

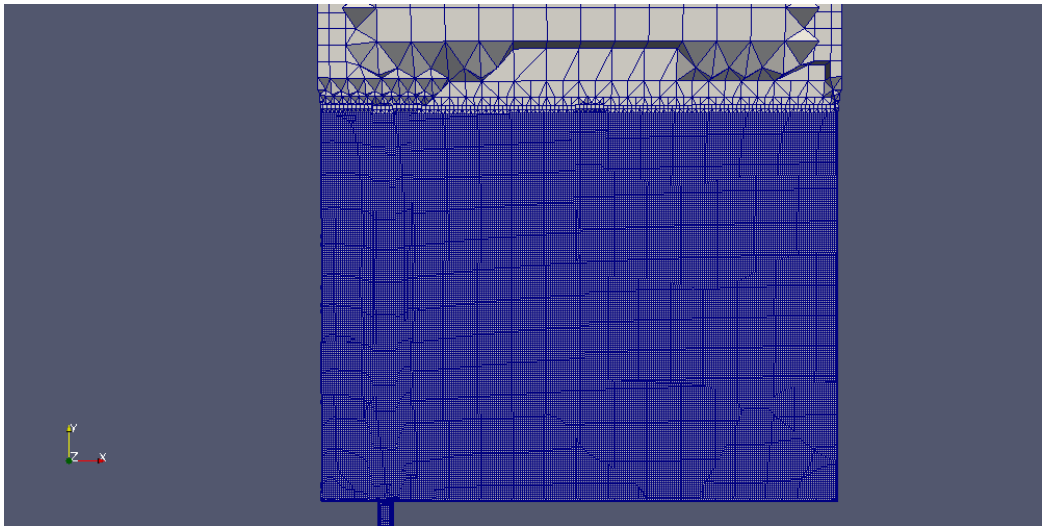

Figure 6.1. Cross-section of the mesh used for this study.

6.1.2 Numerical Methodology

A similar solution methodology to that of the vortex generator study was employed for the jet in cross-flow problem. In order to solve for the turbulent transport of a passive scalar in the jet, an existing solver in OpenFOAM®(pisoFoam) was modified. An additional equation 6.1 was added to be solved at the end of every time step after the calculation of the turbulent viscosity.

$$\frac{\partial c}{\partial t} + u_i \frac{\partial c}{\partial x_i} = \frac{\nu_t}{Sc_t} \nabla^2 u \tag{6.1}$$

Where c is the scalar concentration field, ν_t is the turbulent viscosity that is derived from the turbulence model used and Sc_t is the turbulent Schmidt number. The term $\frac{\nu_t}{Sc_t}$ is the turbulent diffusivity of the passive scalar and it depends on the turbulence model used. Launder [39] and Reynolds [40] talk about the difficulty involved

in selecting the turbulent Schmidt number. Konrad [41] talks about the near wall variation of Sc_t. Tominaga [42] mentions that the optimum values of Sc_t are scattered in the range of $0.2 - 1.3$ and largely depend on the local flow characteristics. It is generally known that the turbulent Schmidt number varies from 0.9 at the wall to 0.6 above the boundary layer. Most commercial flow solvers use a default value of $Sc_t = 0.7$. Hence in this work the turbulent Schmidt number was taken to be 0.7. A $k - \epsilon$ model was used to compare the mean characteristics. Unsteady Navier-Stokes equations were solved using the P.I.S.O algorithm [31]. The convective terms were discretized using a second order upwind scheme while the diffusion terms were discretized with central differencing. Second order implicit Crank-Nicholson scheme was chosen for temporal discretization. The simulation was run till a statistically stationary state was achieved. The side and top walls were given a slip boundary condition as in [2]. The cross-flow was initialized with a Blasius boundary layer profile such that the 80% boundary layer thickness at the center of the jet was equal to $1.32d$. A turbulent plug profile was given to the jet inlet along with a turbulent intensity of 0.5%. The turbulent intensity at the jet inlet was calculated from existing correlations for pipe flows. The velocity at the outlet was given a Dirichlet condition if the velocity flux was directed inside the domain and a Neumann condition if it was directed outside. Pressure at the outlet was fixed at 1 atm. The scalar concentration at the jet inlet was fixed at 1 while it was initialized to be zero in the entire domain including the cross-flow inlet.

6.1.3 Results & Discussion

The jet trajectory was computed using the center plane streamline as in the work of Muppidi [2]. Figure 6.2 shows the computed trajectory along with the

DNS results of [2] and a trajectory scaling law proposed based on experimental investigations.

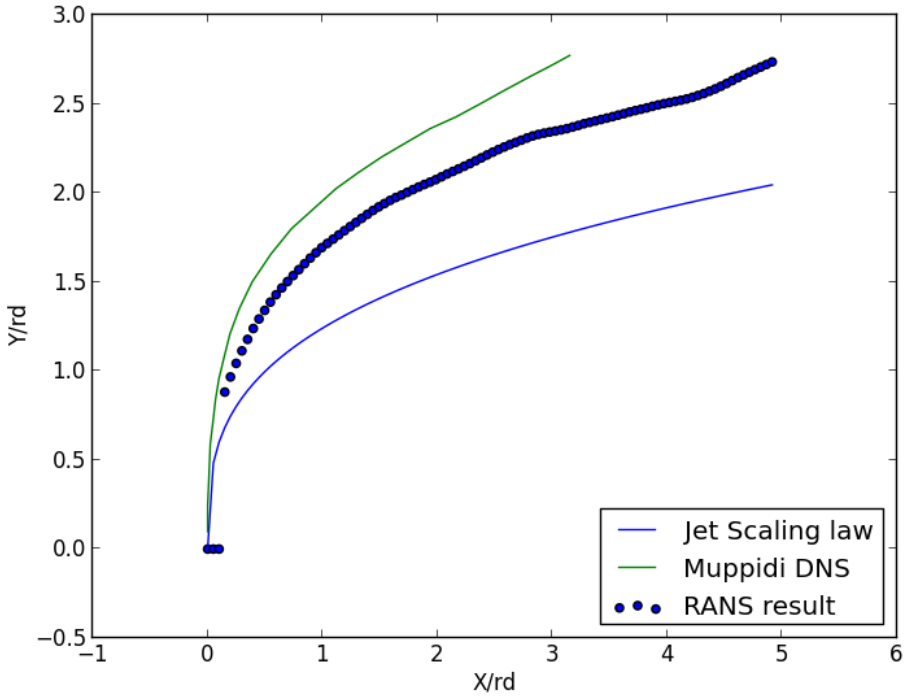

Figure 6.2. Figure showing the jet in cross-flow trajectory.

The RANS predicted trajectory closely matches the DNS results. The difference in the two profiles can be attributed to the fact that a RANS model's assumption of homogeneity adds additional turbulent dissipation and that why the RANS results under predict the trajectory. This is closely related to the fact that not all spatial and temporal scales are resolved well enough. The time instant snapshot of the scalar concentration in the center plane is shown in Figure 6.3.

Figure 6.3. Figure showing the instantaneous center plane scalar concentration.

6.2 Vortex Generator along with Jet in Cross-flow

6.2.1 Computational Domain & Mesh

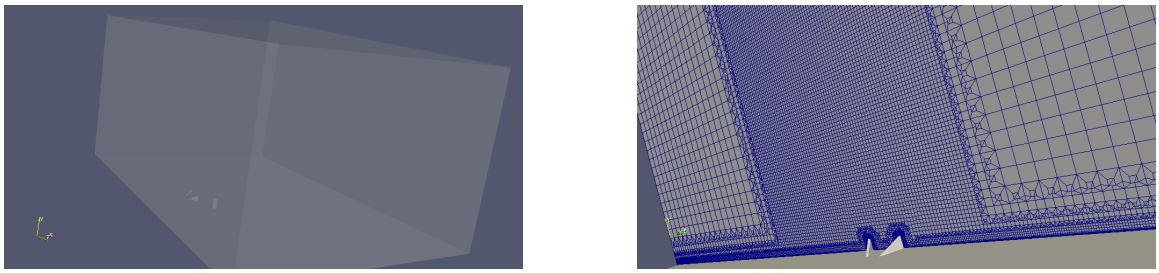

(a) The computational domain (b) Mesh

Figure 6.4. Figure showing the computational domain and mesh for the vortex generator - jet cases.

The computational domain extents considered for this study was the same as that considered for the jet in cross-flow case from above. The vortex generator height and length considered in this study was $h = d$ & $l = 2d$. As for all the previous cases, the macro vortex generator with $\alpha = 30°$ had the highest heat transfer enhancement and thus was chosen for this study. The vortex generator was placed ahead of the jet orifice by a distance $4d$. Wang et al. [28] found that a distance of $4d$ was optimum for their impingement heat transfer enhancement.

The mesh for these cases was also generated in OpenFOAM®. It contained about $4 - 5$ million cells specifically refined around the vortex generator and the jet wake. Figure 6.4 shows a section of the mesh around the vortex generator.

6.2.2 Numerical Methodology

As the jet in cross-flow is an unsteady flow, accurate temporal resolution of the solution is important. Hence a second order implicit Crank-Nicholson scheme was used to discretize the unsteady terms. Similar to the jet in cross-flow methodology, a

second order upwind scheme was used for the convection terms and central differencing was used to discretize the diffusion terms. The solutions were calculated using a piso algorithm.

The left, right and top planes were considered as inviscid walls. Inlet was given a zero pressure gradient condition, inflow velocity condition and the scalar was given a Dirichlet zero boundary condition. The bottom surface, vortex generator and the pipe wall were modeled as no-slip walls. At the outlet the pressure was fixed to 1 atm and velocity and scalar concentration was given a zero gradient boundary condition. The scalar concentration at the jet inlet was fixed at 1 and 0 elsewhere. This helps to isolate and study the decay of the passive scalar along with the jet.

6.2.3 Results & Discussion

All the results were time averaged in order to predict the mean trends.

Figure 6.5 shows the $\lambda 2$ criterion plotted of each of the cases. Similar to the observation of [28], it was observed that the penetration dept of the jet in the cross-flow increases with the use of a Flow-Down configuration ahead of the jet. In order to quantify this increase, the maximum distance that the jet issues into the cross-stream without turning was calculated from the local maximum of center line averaged velocity which was then normalized with the baseline case. It was observed that the penetration depth increases by a factor of 1.094 for the Flow-Down configuration whereas it increases by a factor of 1.26 for the Flow-Up configuration for a velocity ratio of 2.5. For $r = 5.0$, the penetration depth was reduced for the flow-down configuration while that of the flow-up configuration stayed the same.

In order to compare the mixing enhancements of these cases, the mixing efficiency of these configurations were calculated and plotted. The mixing efficiencies were calculated at spanwise planes in the flow direction at a distance of rd - $5rd$

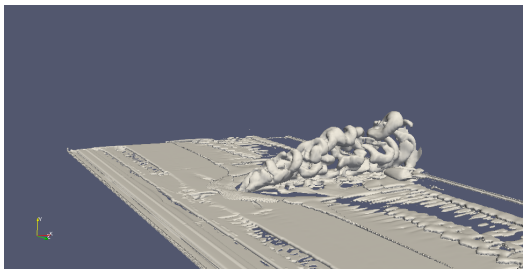

(a) Baseline case of a jet in cross-flow without the vortex generator at $r = 2.5$

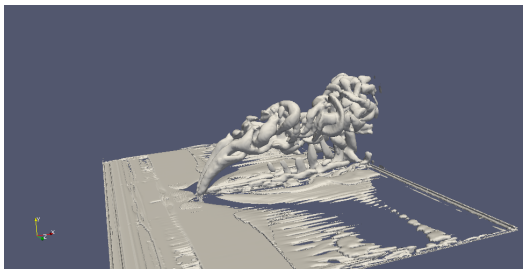

(b) Baseline case of a jet in cross-flow without the vortex generator at $r = 5.0$

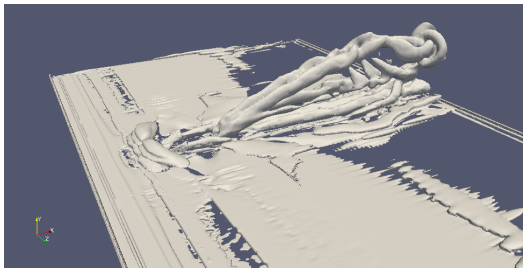

(c) Common Flow-Down configuration of vortex generator at $r = 2.5$

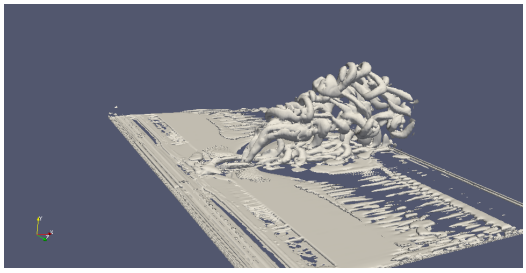

(d) Common Flow-Down configuration of vortex generator at $r = 5.0$

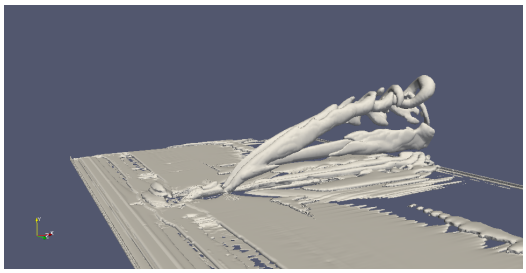

(e) Common Flow-Up configuration of vortex generator at $r = 2.5$

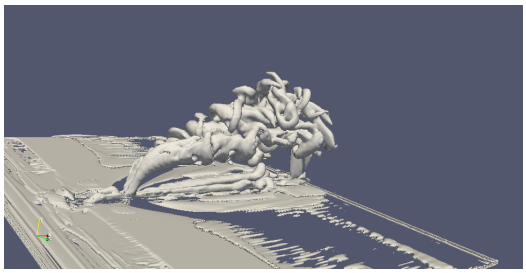

(f) Common Flow-Up configuration of vortex generator at $r = 5.0$

Figure 6.5. Figures showing the $\lambda 2$ criterion to visualize the flow-field.

behind the jet orifice. Here r is the velocity ratio of the jet and d is the jet orifice diameter. The mixing efficiency was defined as the area weighted average of the scalar concentration at these spanwise planes. This was then normalized with the mixing efficiency of the baseline cases at the respective sections. Figure 6.6 shows the streamwise variation of the normalized mixing efficiencies.

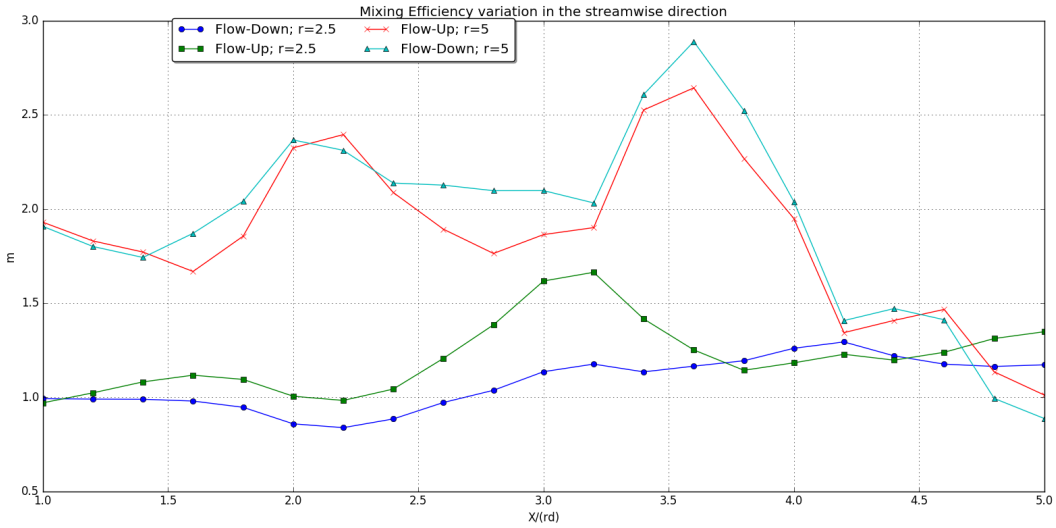

Figure 6.6. Figure showing the normalized mixing efficiency comparison between the Flow-down and Flow-up configurations.

Since all the calculated values were normalized with the baseline cases, the values shown in the figure 6.6 are representative of the enhancement over the jet in cross-flow case.

It was observed that at lower velocity ratio, the flow-up configuration has better mixing performance. A maximum of 60% enhancement was observed. For $r = 5$, the flow-down configuration is slightly better than the flow-up configuration. A maximum enhancement of about 160% was observed for this case.

CHAPTER 7

CONCLUDING REMARKS

7.1 Summary

In this research, the effect of the streamwise vortex strength on the average heat transfer enhancement of the vortex generator was analyzed and a qualitative view of the vortex-boundary layer interaction was presented. The goal was to understand the primary mechanism better, in order to gain physical insight into the enhancement. This would then help us understand the requirements for an efficient design.

The effect of the boundary layer height on the heat transfer enhancement of the vortex generator was studied and was found that the micro vortex generator is less efficient at entraining the colder free-stream fluid and thus has reduced enhancement as compared to the macro vortex generator.

Vorticity transport equation was studied with the goal of identifying the sources and sinks of streamwise vorticity within the longitudinal vortex and the streamwise vorticity contained within the boundary layer. It was observed that the micro vortex generator cases have increased interaction term Φ in the boundary layer vorticity transport that characterizes the entrainment and interaction with the vortex.

The effect of vortex shedding on heat transfer enhancement was analyzed and it was concluded that the periodic shedding also is not conducive to increasing the heat transfer enhancement.

Finally the influence of two of the vortex generator configurations on the mixing enhancement by the jet in cross-flow was investigated. The effect of these configurations on the jet penetration depth was also discussed. The results showed increase

in enhancement of the mixing with the use of the vortex generator. It was observed that the Flow-Up configuration provided better enhancement as compared to the Flow-Down configuration.

7.2 Future Work

- To study the effect of velocity ratio and Schmidt number on the mixing efficiency of the vortex generator - jet configuration.
- Stability analysis of the hybrid enhancement mechanism.
- Flow control of the vortex generator to dampen the vortex shedding.

REFERENCES

[1] A. Jacobi and R. Shah, "Heat transfer surface enhancement through the use of longitudinal vortices: A review of recent progress," *Experimental Thermal and Fluid Science*, vol. 11, no. 3, pp. 295–309, 1995.

[2] S. Muppidi and K. Mahesh, "Direct numerical simulation of round turbulent jets in crossflow," *Journal of fluid mechanics*, vol. 574, pp. 59–84, Mar 2007.

[3] M. Fiebig, P. Kallweit, N. Mitra, and S. Tiggelbeck, "Heat transfer enhancement and drag by longitudinal vortex generators in channel flow," *Experimental Thermal and Fluid Science*, vol. 4, pp. 103–114, 1991.

[4] S. Tiggelbeck, N. Mitra, and M. Fiebig, "Experimental investigations of heat transfer enhancement and flow losses in a channel with double rows of longitudinal vortex generators," *International Journal of Heat and Mass Transfer*, vol. 36, pp. 2327–2337, 1993.

[5] P. Deb, G. Biswas, and N. K. Mitra, "Heat transfer and flow structure in laminar and turbulent flows in a rectangular channel in longitudinal vortices," *International Journal of Heat and Mass Transfer*, vol. 38, pp. 2427–2444, 1995.

[6] M. C. Gentry and A. M. Jacobi, "Heat transfer enhancement by delta-wing vortex generators on a at plate: vortex interactions with the boundary layer," *Experimental Thermal and Fluid Science*, vol. 14, pp. 231–242, 1997.

[7] M. C. Gentry and A. M. Jacobi, "Heat transfer enhancement by delta-wing generated tip vortices in a at-plate and developing channel flows," *ASME Journal of Heat Transfer*, vol. 124, pp. 1158–1168, 2002.

[8] A. Sohankar, "Heat transfer augmentation in a rectangular channel with a vee-shaped vortex generator," *International Journal of Heat and Fluid Flow*, vol. 28, pp. 306–317, 2007.

[9] J. He, L. Liu, and A. Jacobi, "Air-side heat-transfer enhancement by a new winglet-type vortex generator array in a plain-fin round-tube heat exchanger," *ASME Journal of Heat Transfer*, vol. 132, no. 7, pp. 071 801–071 801–9, 2010.

[10] M. Fiebig, "Vortices, generators and heat transfer," *5th UK national Heat Transfer Conference*, vol. 76, no. 2, pp. 108–103, 1998.

[11] A. Abdollahi and M. Shams, "Optimization of shape and angle of attack of winglet vortex generator in a rectangular channel for heat transfer enhancement," *Applied Thermal Engineering*, vol. 81, pp. 376–387, 2015.

[12] L. Salviano, D. Denzen, and J. Yanagihara, "Optimization of winglet-type vortex generator positions and angles in plate-fin compact heat exchanger: Response surface methodology and direct optimization," *International Journal of Heat and Mass Transfer*, vol. 82, pp. 373–387, 2015.

[13] J. Javier and M. Parviz, "The minimal flow unit in near-wall turbulence," *Journal of Fluid Mechanics*, vol. 225, pp. 213–240, April 1991.

[14] J. Marshall, "Cross-stream vorticity field induced by streamwise vortices in unbounded and wall-bounded shear flows," *Theoretical and Computational Fluid Dynamics*, vol. 16, pp. 231–247, Dec 2002.

[15] B. J. Wendt, "Parametric study of vortices shed from airfoil vortex generators," *AIAA Journal*, vol. 42, no. 11, pp. 2185–2195, Nov 2004.

[16] T. Jukes and K. Choi, "On the formation of streamwise vortices by plasma vortex generators," *Journal of Fluid Mechanics*, vol. 733, pp. 370–393, 2013.

[17] M. Krishnan, "The interaction of jets with crossflow," *The Annual Review of Fluid Mechanics*, vol. 45, pp. 379–407, Oct 2012.

[18] D. P. Bruce and W. B. Douglas, "Profiles of the round turbulent jet in a cross flow," *Journal of hydraulics division*, vol. 93, no. 6, pp. 53–64, 1967.

[19] S. Smith and M. Mungal, "Mixing, structure and scaling of the jet in crossflow," *Journal of fluid mechanics*, vol. 357, pp. 83–122, Feb 1998.

[20] L. Su and M. Mungal, "Simultaneous measurements of scalar and velocity field evolution in turbulent crossflowing jets," *Journal of fluid mechanics*, vol. 513, pp. 1–45, Aug 2004.

[21] J. W. Shan and P. E. Demotakis, "Reynolds-number effects and anisotropy in transverse-jet mixing," *Journal of fluid mechanics*, vol. 566, pp. 47–96, Jan 2006.

[22] J. Andreopoulos and W. Rodi, "Experimental investigation of jets in a cross flow," *Journal of fluid mechanics*, vol. 138, pp. 93–127, Jan 1984.

[23] A. R. Karagozian, "An analytical model for the vorticity associated with a transverse jet," *AIAA Journal*, vol. 24, no. 3, pp. 429–436, 1986.

[24] P. Schlatter, S. Bagheri, D. s. Henningson, and P. J. Schmid, "Global stability of a jet in crossflow," *Journal of fluid mechanics*, vol. 624, pp. 33–44, Jan 2009.

[25] A. R. Karagozian, "The jet in crossflow," *Physics of fluids*, vol. 26, no. 10, Sep 2014.

[26] K. B. M. Q. Zaman and J. K. Foss, "The effect of vortex generators on a jet in a crossflow," *Physics of fluids*, vol. 9, no. 1, 1997.

[27] T. Van Buren, E. Whalen, and M. Amitay, "Interaction between a vortex generator and a synthetic jet in a crossflow," *Physics of fluids*, vol. 27, no. 10, 2015.

[28] C. Wang, L. Wang, and B. Sunden, "A novel control of jet impingement heat transfer in cross-flow by a vortex generator pair," *International journal of heat and mass transfer*, vol. 88, pp. 82–90, April 2015.

[29] H. Weller, G. Tabor, H. Jasak, and C. Fureby, "A tensorial approach to computational continuum mechanics using object-oriented techniques," *Computers In Physics*, vol. 12, Nov/Dec 1998.

[30] S. Patankar. Washington: Taylor & Francis, 1980.

[31] R. Issa, "Solution of the implicitly discretized fluid flow equations by operator-splitting," *Journal of Computational Physics*, vol. 62, pp. 40–65, 1985.

[32] P. Roache, K. Ghia, and F. White, "Editorial policy statement on the control of numerical accuracy," *Journal of Fluids Engineering*, vol. 108, no. 2, 1986.

[33] J. M. Wu and W. Q. Tao, "Effect of longitudinal vortex generator on heat transfer in rectangular channels," *Applied Thermal Engineering*, vol. 37, pp. 67–72, 2012.

[34] A. E. Panah, J. M. Akkala, and J. H. J. Buchholz, "Vorticity transport and the leading-edge vortex of a plunging airfoil," *Experiments in Fluids*, vol. 56, pp. 160–175, July 2015.

[35] C. J. Wojcik and J. H. J. Buchholz, "Vorticity transport in the leading-edge vortex on a rotating blade," *Journal of Fluid Mechanics*, vol. 743, pp. 249–261, Jan 2014.

[36] J. Jeong and F. Hussain, "On the identification of a vortex," *Journal of Fluid Mechanics*, vol. 285, pp. 69–94, 1995.

[37] S. Camarri and A. Lollo, "Feedback control of the vortex shedding instability based on sensitivity analysis," *Physics of Fluids*, vol. 22, no. 094102, September 2010.

[38] M. Sheikholeslami, M. Gorji-Bandpy, and D. Domiri Ganji, "Review of heat transfer enhancement methods: Focus on passive methods using swirl flow devices," *Renewable and Sustainable Energy Reviews*, vol. 49, pp. 444–469, September 2015.

[39] B. Launder. Berlin: Springer, 1976.

[40] A. Reynolds, "The prediction of turbulent prandtl and schmidt numbers," *International journal of heat and mass transfer*, vol. 18, pp. 1055–1069, Sept. 1975.

[41] K. Konrad, "The height dependence of the turbulent schmidt number within the boundary layer," *Atmospheric environment*, vol. 34, no. 7, pp. 1147–1151, 2000.

[42] Y. Tominaga and T. Stathopoulos, "Turbulent schmidt numbers for cfd analysis with various types of flowfield," *Atmospheric environment*, vol. 41, no. 37, pp. 8091–8099, Dec 2007.

BIOGRAPHICAL STATEMENT

Aditya Raman was born in the city of Mumbai, India 1989. He obtained his bachelors degree in Mechanical Engineering from D.Y. Patil College of Engineering, University of Pune in 2010. He came to US in 2011 to pursue a PhD in Aerospace Engineering under the guidance of Dr Brian Dennis.

His research interests include fluid dynamics and heat transfer, vortex-boundary layer interactions, vortex shedding, flow instability and control, spectral/h-p element methods and immersed boundary methods. He has been a Graduate Teaching Assistant at UTA since 2012. He is a student member of AIAA and ASME.